

OPTICAL ANALYSIS AND OPTIMIZATION OF
LINE FOCUS SOLAR COLLECTORS

P. BENDT
A. RABL
H. W. GAUL
K. A. REED

SEPTEMBER 1979

PREPARED UNDER TASK NO. 3432.30

Solar Energy Research Institute

1536 Cole Boulevard
Golden, Colorado 80401

A Division of Midwest Research Institute

Prepared for the
U.S. Department of Energy
Contract No. EG-77-C-01-4042

Printed in the United States of America
Available from:
National Technical Information Service
U.S. Department of Commerce
5285 Port Royal Road
Springfield, VA 22161
Price:
Microfiche \$3.00
Printed Copy \$5.25

NOTICE

This report was prepared as an account of work sponsored by the United States Government. Neither the United States nor the United States Department of Energy, nor any of their employees, nor any of their contractors, subcontractors, or their employees, makes any warranty, express or implied, or assumes any legal liability or responsibility for the accuracy, completeness or usefulness of any information, apparatus, product or process disclosed, or represents that its use would not infringe privately owned rights.

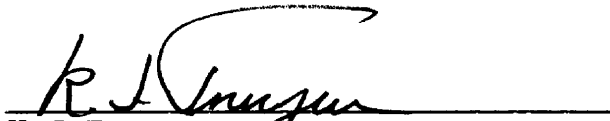
FOREWORD

This report was prepared under Contract No. EG-77-C-01-4042, SERI Task 3432.30, by P. Bendt, A. Rabl, and H. W. Gaul of the Thermal Conversion Branch of the Solar Energy Research Institute, and by K. A. Reed of Argonne National Laboratory. The authors thank F. Biggs, D. F. Grether, A. Hunt, K. Masterson, and G. W. Treadwell for helpful discussions.



Frank Kreith
Branch Chief
Thermal Conversion Branch

Approved for:
SOLAR ENERGY RESEARCH INSTITUTE



K. J. Touryan
Acting Assistant Director
for Research

SUMMARY

The optical analysis of a solar concentrator is usually carried out by means of computer ray tracing, a microscopic method that provides an enormous amount of detailed information but obscures functional relationships. This paper describes a macroscopic approach that yields all the parameters needed for the optical design of line focus parabolic troughs in closed analytical form, requiring only minimal computation.

The goal of the optical analysis developed in this report is to determine the flux at the receiver as a function of concentrator configuration, receiver size, width of sun, and optical errors (e.g., tracking, reflector contour). All causes of image spreading are quantified as angular standard deviation. Ray tracing with a real reflector and a real sun is shown to be equivalent to convoluting the angular acceptance function of a perfect concentrator with an effective radiation source. This effective source, in turn, is obtained by convoluting the distribution function of optical errors with the angular profile of the sun. The problem is reduced to two dimensions by projecting the three-dimensional motion of the sun on the plane normal to the tracking axis. In this frame the apparent width of the sun increases as $1/\cos \Theta$ with incidence angle Θ .

A formula is derived for the optimal geometric concentration ratio, maximizing net power output as a function of all relevant variables (all-day average insolation, optical errors, effective transmittance-absorptance, heat loss, and concentrator configuration). Graphical solution of this equation consists of finding the intersection between a universal curve and a straight line representing a critical intensity ratio.

In the last section, which is written as a self-contained users guide, the results are summarized and illustrated by specific examples.

TABLE OF CONTENTS

	<u>Page</u>
Nomenclature	xiii
1.0 Introduction	1
2.0 Two-Dimensional Projection	3
2.1 Projection of Ray-Trace Diagram	3
2.2 Projection of Position of Sun.....	6
2.3 Projection of Optical Errors	9
3.0 Calculation of Flux at Receiver	13
3.1 Effective Source	13
3.2 Angular Acceptance Function.....	16
3.3 Flux at Receiver and Intercept Factor	20
4.0 Approximation of Sun Shape by Gaussian Distribution	23
5.0 Optimal Concentration Ratio	33
6.0 Examples/Users Guide	41
6.1 Optimization Philosophy	41
6.2 Collector Parameters	42
6.3 Choice of Rim Angle	44
6.4 Optimization of Concentration Ratio	44
6.5 Calculation of Intercept Factor and Operating Efficiency	50
6.6 Sensitivity of Optimization to Changes in Collector Parameters.....	53
6.7 Sensitivity to Circumsolar Radiation.....	53
6.8 Operation with North-South Axis	55
7.0 References	57
Appendix: Typical Insolation Values for Use in Optimization.....	59

LIST OF FIGURES

	<u>Page</u>
2-1 Definition of Coordinates and Projected Incidence Angles (a) Θ_{\perp} and (b) Θ_{\parallel} for Two-Dimensional Concentrators	4
2-2 Projected Ray-Trace Diagram for Troughlike Reflector Is Independent of Elevation of Incident Ray from x-y Plane.....	5
2-3 Position of Sun Relative to Line Focus Concentrator at Noon and in Morning or Afternoon	7
2-4 Definition of Mirror Contour Error Angular Variables $d\vec{\omega}_{\parallel}$ and $d\vec{\omega}_{\perp}$	10
3-1 Equivalence Between (a) Imperfect Reflector with Point Source and (b) Perfect Reflector with Smeared Source	14
3-2 (a) Geometric Relations for the Calculation of the Angular Acceptance Function.....	17
(b) Angular Acceptance Function for $\Phi = 90^{\circ}$ Trough with Cylindrical Receiver (Schematic)	19
(c) Angular Acceptance Function for $\Phi = 45^{\circ}$ Trough with Flat Receiver (Schematic)	19
4-1 Intercept Factor γ Versus $\sigma_{tot} C$ for Different Rim Angles Φ (Gaussian Approximation) for	
(a) Cylindrical Receiver.....	24
(b) Flat Receiver.....	25
4-2 Intercept Factor γ Versus $1/C$ for	
(a) Circumsolar Scan Number 1 (Narrow)	26
(b) Circumsolar Scan Number 11 (Wide)	27
(c) Circumsolar Scan Number 16 (Very Wide).....	28
(d) Average over Circumsolar Scans 1 through 10	29
5-1 The Curve $G(\sigma_{tot} C)$ for Finding the Optimal Concentration Ratio for Different Rim Angles Φ for	
(a) Cylindrical Receiver.....	38
(b) Flat Receiver.....	39
6-1 Intercept Factor γ Versus Rim Angle for Parabolic Trough with	
(a) Cylindrical Receiver.....	45
(b) Flat Receiver.....	46

LIST OF TABLES

	<u>Page</u>
2-1 Quantities Needed for Evaluation of Transverse Effects of Longitudinal Contour Errors in Parabolic Trough with East-West Tracking Axis.....	11
4-1 Parameters for the 16 Standard LBL Circumsolar Scans	31
5-1 Optimization of Concentration Ratio for Real Sun and for Gaussian Sun	36
6-1 Collector Parameters	43
6-2 Tracking Modes and Associated Solar Data.....	47
6-3 Optimization of Concentration Ratio for Parabolic Trough with East-West Axis: Worksheet	49
6-4 Calculation of Efficiency for Collector Optimized According to Table 6-3: Worksheet.....	52
6-5 Sensitivity of Optimization to Change in Heat Loss Parameter q_L	53
6-6 Sensitivity to Circumsolar Radiation, Exact Calculation and Gaussian Approximation. Intercept Factor γ as Function of $\sigma_{optical}$ and C (For $\phi = 90^\circ$)	54
6-7 Calculation of Efficiency of Collector with C = 27.3 (Optimized for East-West Axis) If Operated with Horizontal North-South Axis.....	56
A-1 Average of Cosine Factors for Collector with East-West Tracking Axis	63

NOMENCLATURE

The optimization procedure proposed in this paper is based on typical all-day average values of insolation. All-day averages are designated by angular brackets $\langle \rangle$. A subscript t_c under the bracket indicates that the average is taken over an operating period from t_c hours before until t_c hours after solar noon. Subscripts \parallel and \perp designate angular variables measured parallel or transverse to the tracking axis.

$B_{\text{sun}}(\Theta)$	Angular profile of sun ($\text{W}/\text{m}^2 \text{ rad}$) for line focus geometry
$B_{\text{eff}}(\Theta)$	Effective source ($\text{W}/\text{m}^2 \text{ rad}$) = convolution of solar profile $B_{\text{sun}}(\Theta)$ and distribution function $E(\Theta)$ of optical errors
C	Geometric concentration ratio = ratio of aperture area over receiver surface area (For example, a trough of aperture width D and receiver tube diameter d has $C = D/(\pi d)$.)
C_o	Optimal concentration ratio
D	Aperture width
d	Absorber diameter
$E(\Theta)$	Distribution function of optical errors (rad^{-1})
$f(\Theta)$	Angular acceptance function = fraction of rays incident on aperture at incidence angle Θ from optical axis that reach receiver
$G(\sigma C)$	Function used for optimizing C
H_d	Daily total diffuse irradiation on horizontal surface (J/m^2)
H_h	Daily total hemispherical irradiation on horizontal surface (J/m^2)
H_o	Daily total extraterrestrial irradiation on horizontal surface (J/m^2)
I_b	Beam component of solar irradiance (W/m^2) as measured by pyrheliometer (also known as direct normal insolation)
$\langle I_b \cos \Theta \rangle$	Day-long average beam irradiance on collector aperture (including cosine factor)
I_d	Diffuse component of solar irradiance, assumed to be isotropic (W/m^2)
I_h	Hemispherical irradiance on horizontal surface

I_o	Solar constant = 1353 W/m^2
K_h	$H_h/H_o =$ clearness index
q_{in}	That portion of I_b that would reach the receiver (W per m^2 of aperture area) if $(\rho \tau \alpha)$ were equal to one
q_L	$Cq_{loss} =$ heat loss (W/m^2) per receiver surface area
q_{net}	$(\rho \tau \alpha) q_{in} - q_{loss} =$ power output of collector (W per m^2 of aperture area)
$q_{shading}$	That portion of I_b prevented from reaching receiver because of shading of aperture by receiver
r_d	$I_d/H_d =$ conversion from irradiance to daily irradiation for the diffuse component
r_h	$I_h/H_h =$ conversion from irradiance to daily irradiation for the hemispherical component
t	Time of day (from solar noon)
t_c	Collector cutoff time
t_s	Sunset time
X	$X_S + \left(\frac{q_L}{(\rho \tau \alpha)} - I_d \right) / I_b =$ critical intensity ratio
X_S	Contribution of shading term to critical intensity ratio
α	Absorptance of receiver
γ	$q_{in}/I_b =$ intercept factor
γ_{Gauss}	Intercept factor if sun is approximated by Gaussian distribution
$\gamma(\theta_{\perp})$	Intercept factor if collector is misaligned; that is, with its optical axis pointing an angle θ_{\perp} away from the sun
δ	Declination
η	$q_{net}/I_b =$ collector efficiency
η_o	Optical efficiency = $(\rho \tau \alpha)\gamma$
θ	Incidence angle

θ_h	Incidence angle on horizontal surface
λ	Geographic latitude
$\lambda(\phi)$	Rim-angle-dependent contribution of longitudinal mirror errors to transverse beam spreading
$(\rho \tau \alpha)$	Effective reflectance-transmittance-absorptance product of collector
σ_{contour}	rms angular deviation of contour from design direction
$\sigma_{\text{displacement}}$	Equivalent rms angular spread which accounts for imperfect placement of receiver
σ_{specular}	rms spread of reflected beam due to imperfect specularity of reflector material
σ_{optical}	rms angular spread caused by all optical errors
σ_{sun}	rms angular width of sun in line focus geometry
σ_{tot}	Total rms beam spread
τ	Transmittance of collector glazing, if any
ϕ	Rim angle
ϕ_o	Optimal rim angle
ω	$2 \pi t/T =$ hour angle
ω_c	$2 \pi t_c/T =$ collector cutoff angle
ω_s	$2 \pi t_s/T =$ sunset hour angle

SECTION 1.0

INTRODUCTION

Traditionally the optical analysis of solar concentrators has been carried out by means of computer ray-trace programs [1-3]. Ray tracing is a microscopic method which can provide an enormous amount of detailed information but obscures functional relationships. Recognition of functional relationships is of utmost importance for the development of simplified design procedures. This paper shows how all the relevant parameters for the optical design of line focus solar concentrators can be obtained by a simple macroscopic approach. It is shown in most cases that approximations are permissible whereby all quantities of interest can be determined from a few graphs. This paper deals explicitly with parabolic troughs, but much of the analysis is applicable to other line focusing collectors as well.

Treatment of optical properties in isolation is justified because, to an excellent approximation, the optical and the thermal behaviors of solar collectors are independent of each other.* In the optimization of the concentrator the thermal properties enter only through a single parameter q_L , the heat loss per unit receiver surface. In Section 2.0 the optical problem is reduced from three to two dimensions by projecting all rays onto the plane normal to the tracking axis. In this frame the apparent size of the sun increases with incidence angle Θ as $1/\cos \Theta$. The effect of longitudinal mirror errors on this projection is evaluated; it increases with rim angle Φ but even at $\Phi = 90^\circ$ it is small. In Section 3.0 ray tracing is shown to be equivalent to convoluting an effective source function with the angular acceptance function of the concentrator. It is convenient to calculate the angular acceptance function for perfect optics and to include errors in the effective source. The effective source is obtained by convoluting the solar profile with the distribution function of optical errors, and in most cases it can be replaced by a Gaussian distribution. This step, henceforth referred to as Gaussian approximation, is motivated by the central limit theorem of statistics.** It is attractive because it reduces the number of independent parameters. The difference between the intercept factors calculated with the real sun and with the Gaussian approximation is evaluated in Section 4.0, using the circumsolar data supplied by the Lawrence Berkeley Laboratory [5]. Only for collectors with relatively low optical errors is the difference significant. In Section 5.0 the optimal concentration ratio, i.e., the ratio of aperture to receiver surface area, is calculated for thermal collectors by maximizing the efficiency. The optimum is broad enough to permit determination with the Gaussian approximation in all cases of interest. The optimization procedure consists of finding the

* Warming of the receiver enclosure by direct absorption of solar radiation can reduce heat losses, but this effect can be treated as a shift in the optical efficiency (see Section 7.9 of Ref. 14) and we shall assume it to be included in the effective $(\rho\tau\alpha)$ product.

** See, for example, Reference 4.

intersection of a straight line, corresponding to a critical intensity ratio, with a universal curve. The optimal rim angle ϕ_o is shown to be in the range 90° to 120° for a parabolic trough with cylindrical receiver and 45° to 60° for a flat receiver. Near the optimum the efficiency is so insensitive to ϕ that the choice of rim angle can be based entirely on other considerations, such as the structural strength and ease of manufacturing.

Readers who are not interested in the technical details are advised to proceed directly to Section 6.0 where the results are summarized and illustrated by specific examples. First, the optimal concentration ratio of a parabolic trough with cylindrical receiver and 90° rim angle is calculated for specified values of optical errors and heat loss. (The optimization is based on a typical long-term average insolation value [6], integrated over time of day, as calculated in the Appendix.) The resulting peak and all-day average efficiencies are then calculated. The sensitivity of the optimization to changes in collector parameters and operating conditions is evaluated, particularly with regard to circumsolar radiation.

SECTION 2.0

TWO-DIMENSIONAL PROJECTION

For the following discussion it is convenient to choose a coordinate system in which the z axis is placed along the tracking axis and the y axis along the axis of symmetry or optical axis, as shown in Figure 2-1. Θ_{\perp} and Θ_{\parallel} are the projections of the incidence angle of the sun on the x-y plane and on the y-z plane, respectively. With perfect tracking the misalignment angle Θ_{\perp} vanishes and Θ_{\parallel} equals the incidence angle.

2.1 PROJECTION OF RAY-TRACE DIAGRAM

First, the law of specular reflection is stated in vector notation in terms of the following unit vectors:

$$\begin{aligned} \hat{i} &= \text{direction of incident ray,} \\ \hat{n} &= \text{direction of normal of reflector surface, and} \\ \hat{r} &= \text{direction of reflected ray.} \end{aligned}$$

All three vectors point away from the surface.

For given \hat{i} and \hat{n} the direction of the reflected ray is

$$\hat{r} = -\hat{i} + 2(\hat{i} \cdot \hat{n})\hat{n}. \quad (2-1)$$

Next, a particular ray which hits the reflector with angle of incidence Θ_i is traced. The projections $\Theta_{i,xy}$ and $\Theta_{r,xy}$ of the angles of incidence Θ_i and reflection Θ_r on the x-y plane, shown in Figure 2-2, are given by

$$\cos \Theta_{i,xy} = \hat{i}_{xy} \cdot \hat{n}_{xy} = i_x n_x + i_y n_y = \hat{i} \cdot \hat{n} - i_z n_z \quad (2-2a)$$

and

$$\cos \Theta_{r,xy} = \hat{r}_{xy} \cdot \hat{n}_{xy} = r_x n_x + r_y n_y = \hat{r} \cdot \hat{n} - r_z n_z. \quad (2-2b)$$

They are equal if n_z vanishes. Thus, in any troughlike reflector aligned along the z axis, all incident rays with the same x-y projection (plane of the paper in Fig. 2-2) are represented by the same two-dimensional ray-trace diagram, no matter how large their elevation Θ_{\parallel} from the x-y plane.

Therefore, rays with the same x,y components but different z components need not be traced separately. If a planar ray entering with $\hat{i} = (i_x, i_y, 0)$ has been found to leave in the direction $\hat{s} = (s_x, s_y, 0)$, then a nonplanar ray entering with

$$\hat{i}' = \left(i_x \sqrt{1 - (i_z')^2}, \quad i_y \sqrt{1 - (i_z')^2}, \quad i_z' \right), \quad (2-3)$$

i_z' being arbitrary, has the same x-y projection and leaves with

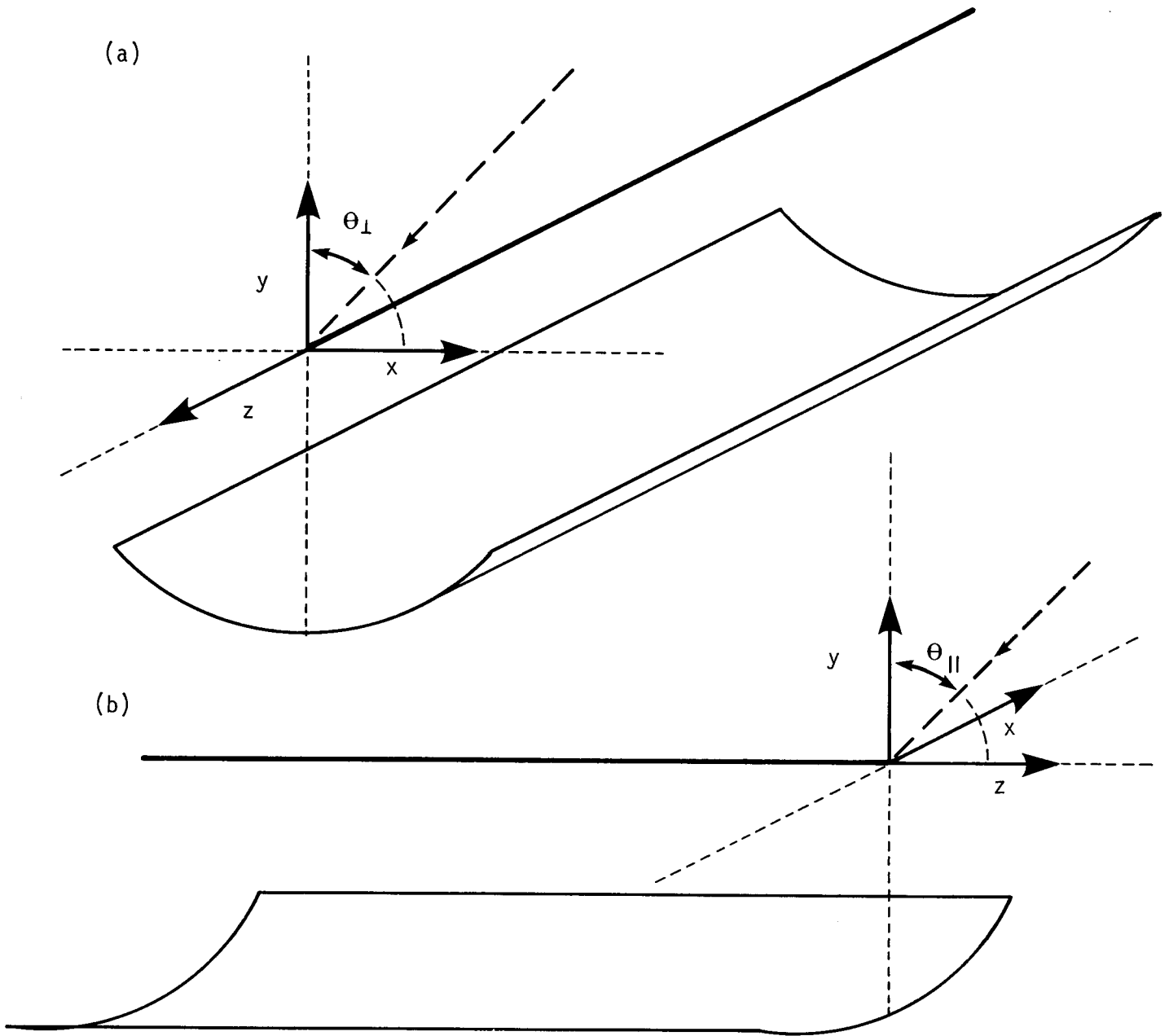


Figure 2-1. DEFINITION OF COORDINATES AND PROJECTED INCIDENCE ANGLES
(a) θ_{\perp} AND (b) θ_{\parallel} FOR TWO-DIMENSIONAL CONCENTRATORS.

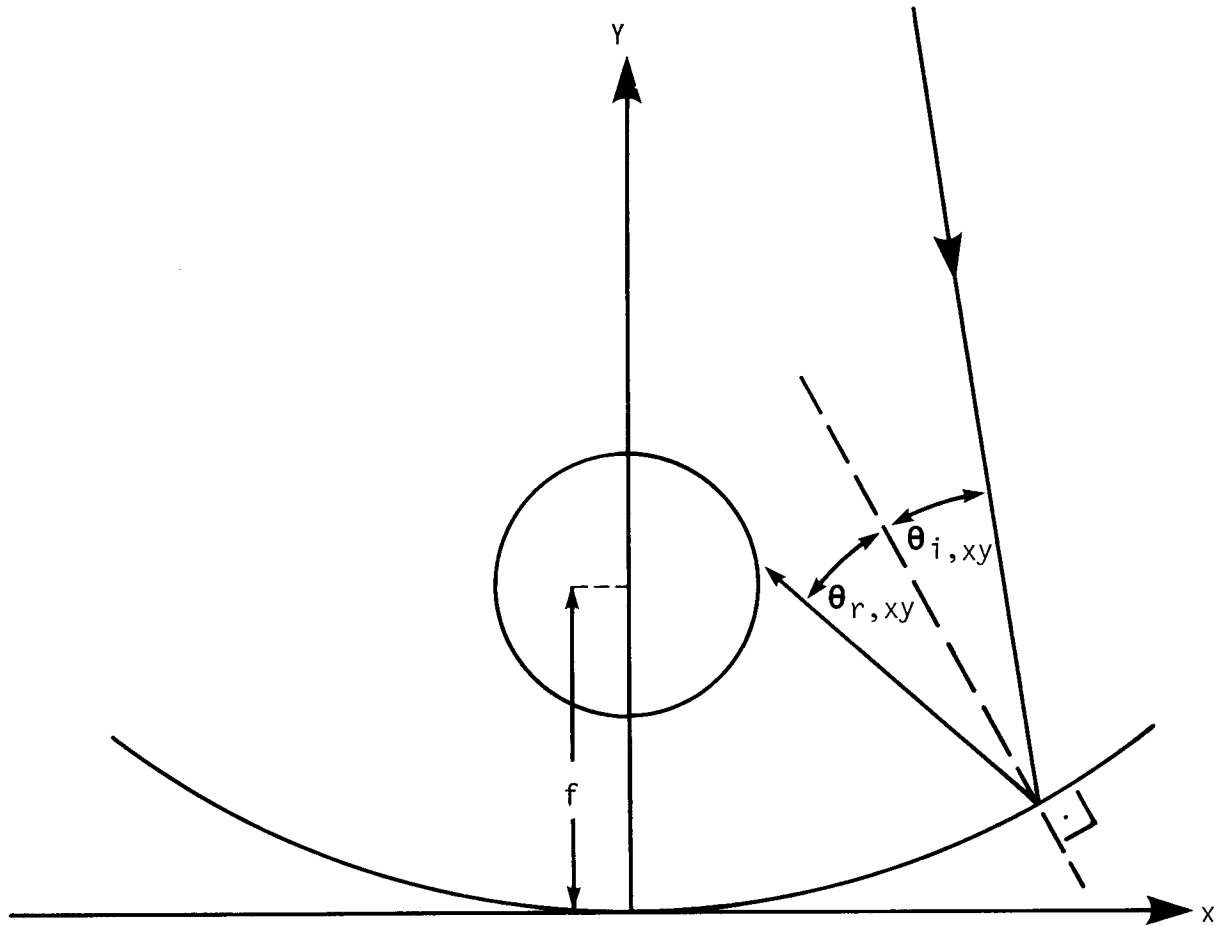


Figure 2-2. PROJECTED RAY-TRACE DIAGRAM FOR TROUGHLIKE REFLECTOR IS INDEPENDENT OF ELEVATION OF INCIDENT RAY FROM x - y PLANE.

$$\hat{s}' = \left(s_x \sqrt{1 - (i'_z)^2}, s_y \sqrt{1 - (i'_z)^2}, i'_z \right). \quad (2-4)$$

This implies that in troughlike reflectors the ray-trace diagram and, in particular, the focal length are independent of the elevation of the incident ray from the x-y plane [7].*

2.2 PROJECTION OF POSITION OF SUN

When a line focus concentrator is employed as a solar collector, the elevation of the sun from the x-y plane does have an effect** on the width of the image on the receiver. Within a two-dimensional analysis this can be explained by the following argument. In the frame of the earth the sun moves in a circle, and it is this circular motion which breaks the translational symmetry of a line focus reflector. This is shown schematically in Figure 2-3. At noon the sun is in the x-y plane and the angular half-width Δ_s of the solar disc (note $\Delta_s \ll 1$) is

$$\Delta_s = \frac{r}{R}, \quad (2-5)$$

with r = radius of the solar disc and R = distance from the earth to the sun.

In the reference frame of the collector the apparent diurnal motion of the sun is a circle of radius R around the earth; therefore, away from solar noon, the projected angular half-width of the sun in the x-y plane is

$$\Delta_{s,xy} = \frac{r}{R_{xy}} = \frac{\Delta_s}{\cos \Theta_{||}}, \quad (2-6)$$

where R_{xy} is the projection

$$R_{xy} = R \cos \Theta_{||} \quad (2-7)$$

of the sun-to-earth distance on the x-y plane. This is the projected angular width which must be used as input in the two-dimensional ray-trace diagram, and hence the width of the solar image on the receiver varies as $1/\cos \Theta_{||}$. For a concentrator with east-west axis, the effective angular width of the sun at four hours from noon will be twice as large as at noon. For tracking polar-mounted concentrators, on the other hand, $\Theta_{||}$ equals the solar declination δ , and this effect can probably be neglected because $\cos \delta$ is always larger than 0.92. For collectors with horizontal north-south tracking axes, however, this

*This contrasts with linear refractive concentrators for which the focal lengths change with nonnormal incidence.

**In troughs of finite length there is an obvious additional effect which is design dependent. This effect is the loss of radiation from the ends of the reflectors. It can be minimized by using end reflectors, long troughs, or polar mounts.

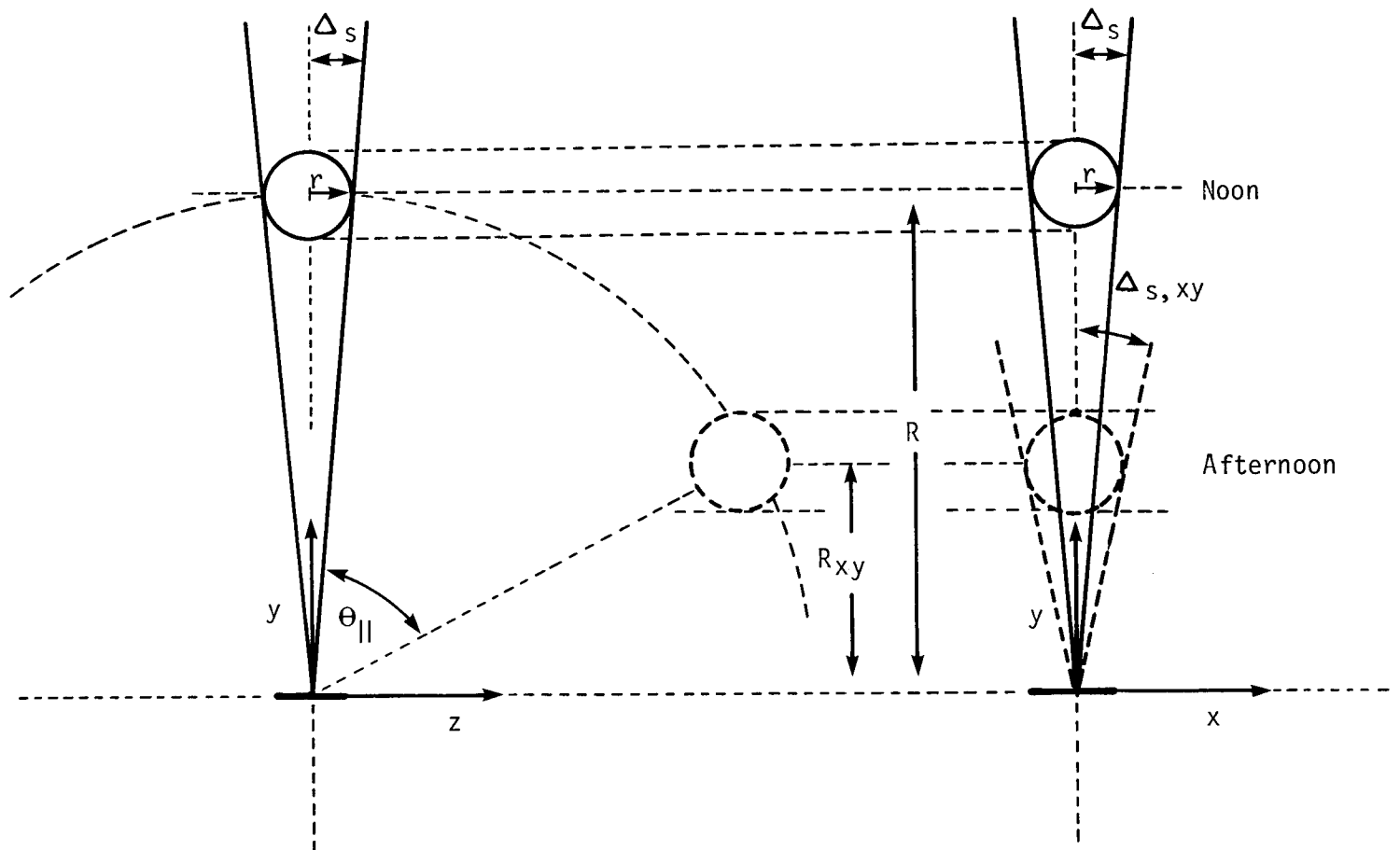


Figure 2-3. POSITION OF SUN RELATIVE TO LINE FOCUS CONCENTRATOR AT NOON AND IN MORNING OR AFTERNOON.

image spread can cause serious problems at latitudes λ far from the equator. Not only is the image enlarged by a factor $1/\cos(\lambda + \delta)$, but the summer-to-winter variation yields the widest image and hence the lowest intercept factor at a time when the insolation is also at its minimum.

The variability of the projected solar size raises the question of which value should be chosen as the basis for concentrator design. An all-day average of the standard deviation σ_{sun} , weighted by the available beam insolation $I_b \cos \Theta_{||}$, appears reasonable:

$$\langle \sigma_{\text{sun}}^2 \rangle = \frac{\int_{-t_c}^{t_c} dt I_b(t) \cos \Theta_{||} \left(\frac{\sigma_{\text{sun,noon}}}{\cos \Theta_{||}} \right)^2}{\int_{-t_c}^{t_c} dt I_b(t) \cos \Theta_{||}} \quad (2-8)$$

$\Theta_{||} = \Theta_{||}(t)$ is the angle of incidence at time-of-day t , and the collector is assumed to operate from t_c hours before until t_c hours after solar noon. Since it will become clear shortly that σ_{sun}^2 is rather insensitive to any details of the averaging procedure, the next step is to consider equinox when $\Theta_{||}$ for the east-west case equals the hour angle

$$\omega = \frac{2\pi t}{T}, \quad T = 24 \text{ h,}$$

and

$$\langle \sigma_{\text{sun}}^2 \rangle = \sigma_{\text{sun,noon}}^2 \frac{\int_0^{\omega_c} d\omega I_b(\omega) / \cos \omega}{\int_0^{\omega_c} d\omega I_b(\omega) \cos \omega} \quad (2-9)$$

The long-term average dependence of $I_b(\omega)/I_b(0)$ on hour angle ω is certainly bounded by one and $\cos \omega$ (for a more precise analysis see the Appendix). Choosing $t_c = 4$ h as a typical value we find

$$\langle \sigma_{\text{sun}}^2 \rangle = 1.52 \sigma_{\text{sun,noon}}^2, \quad \text{with } I_b(\omega) = I_b(0) \cos \omega \quad (2-10)$$

and

$$\langle \sigma_{\text{sun}}^2 \rangle = 1.41 \sigma_{\text{sun,noon}}^2, \quad \text{with } I_b(\omega) = I_b(0) \cos^2 \omega. \quad (2-11)$$

This leads to the recommendation of

$$\langle \sigma_{\text{sun}}^2 \rangle = 1.5 \sigma_{\text{sun,noon}}^2 \quad (2-12)$$

as a reasonable rule for incorporating time-of-day effects into the projected size of the sun for line focus collectors with east-west tracking axes.

2.3 PROJECTION OF OPTICAL ERRORS

In this section the effect of local contour errors in the mirror are treated first, followed by a discussion of concentrator tracking errors. It is assumed that contour errors can be analyzed as if they manifested themselves as rotations but not displacements of elemental surface areas, giving rise to a rotation of the unit surface normal \hat{n} at a point of reflection. The contour error can then be described in terms of two angular variables, $d\vec{\omega}_{\perp}$ and $d\vec{\omega}_{\parallel}$, which lead to rotations of \hat{n} in the planes perpendicular and parallel to the trough axis, respectively. As shown in Figure 2-4, $d\vec{\omega}_{\perp} = d\omega_{\perp} \hat{z}$ and $d\vec{\omega}_{\parallel}$ are orthogonal to \hat{n} and to each other. The change in the unit normal is

$$d\vec{n} = d\vec{n}_{\perp} + d\vec{n}_{\parallel} \quad (2-13a)$$

$$= \hat{n} \times d\vec{\omega}_{\perp} + \hat{n} \times d\vec{\omega}_{\parallel} \quad (2-13b)$$

$$= (n_y d\omega_{\perp}, -n_x d\omega_{\perp}, -d\omega_{\parallel}), \quad (2-13c)$$

assuming \hat{n} lies in the x-y plane. The change in the reflected ray is found by differentiation of Eq. 2-1:

$$d\vec{r} = 2(\hat{i} \cdot d\vec{n})\hat{n} + 2(\hat{i} \cdot \hat{n})d\vec{n}. \quad (2-14)$$

The quantity sought is the change in the angle of reflection projected on the x-y plane, $d\Theta_{r,xy}$ (Figure 2-2), or, for brevity, $d\Theta$. Inverting the relation

$$d\vec{r} = \vec{r} \times d\vec{\Theta} \quad (2-15)$$

produces the desired result:

$$d\Theta = \frac{r_y dr_x - r_x dr_y}{(r_x^2 + r_y^2)}. \quad (2-16)$$

Substituting the necessary components from Eqs. 2-1 and 2-14, setting $i_x = 0$, and recognizing that $i_z/i_y = \tan \Theta_{\parallel}$, one obtains the final result

$$d\Theta = 2d\omega_{\perp} + 2n_x \tan \Theta_{\parallel} d\omega_{\parallel}. \quad (2-17)$$

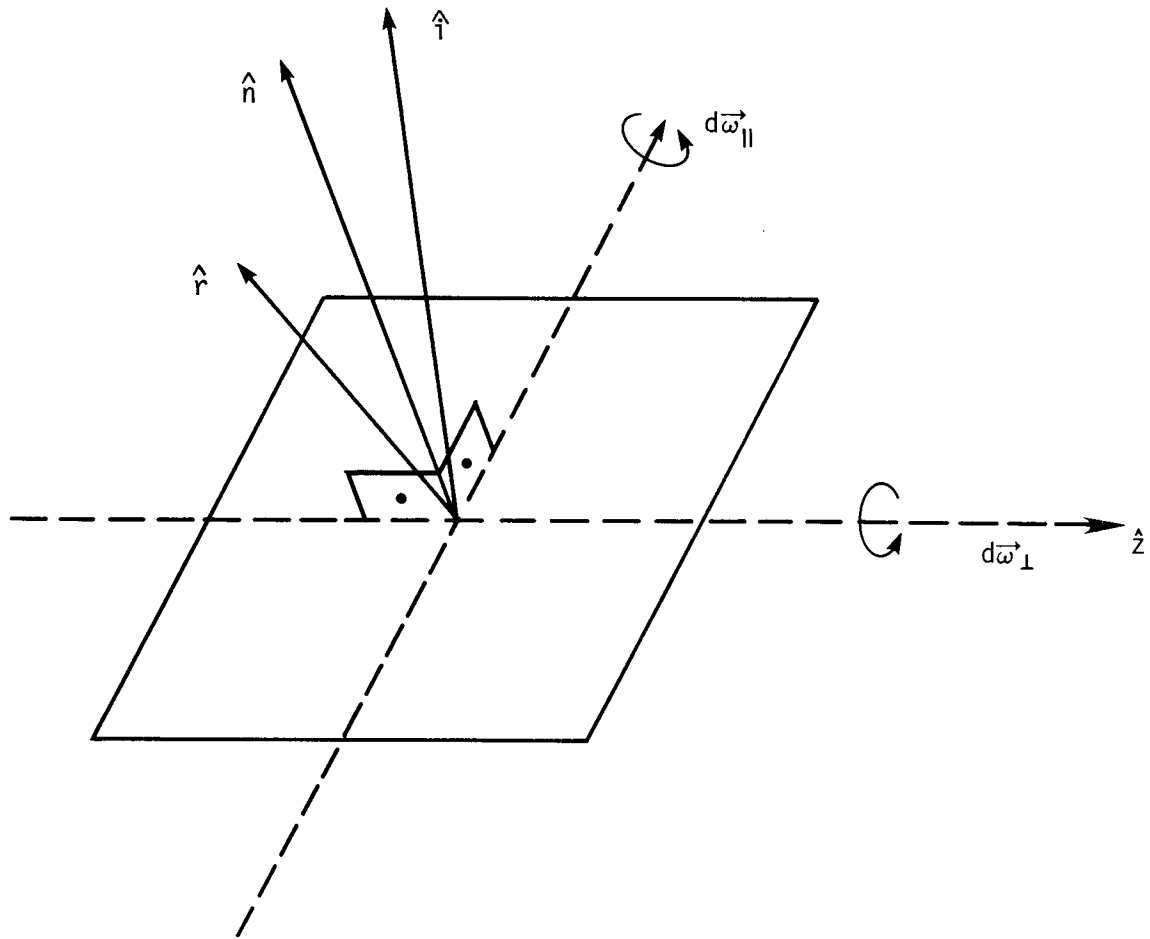


Figure 2-4. DEFINITION OF MIRROR CONTOUR ERROR ANGULAR VARIABLES $d\vec{\omega}_{\parallel}$ AND $d\vec{\omega}_{\perp}$.

If the distributions of mirror contour errors $d\omega_{\perp}$ and $d\omega_{\parallel}$ are independent and described respectively by standard deviations $\sigma_{\text{contour}_{\perp}}$ and $\sigma_{\text{contour}_{\parallel}}$, the distribution in projected angle will be described by the variance

$$\sigma^2 = 4 \sigma_{\text{contour}_{\perp}}^2 + 4n_x^2 \tan^2 \Theta_{\parallel} \sigma_{\text{contour}_{\parallel}}^2 \quad (2-18)$$

The transverse angular spread resulting from longitudinal contour errors is seen to depend on the time of day (via Θ_{\parallel}) and on the incidence point of radiation on the aperture (via n_x^2); a rigorous ray-trace analysis of a parabolic trough should be based on Eq. 2-18. On the other hand, for the formalism developed in this paper it is desirable to replace this equation with a single effective contour error which is averaged over aperture and over time of day. Such averaging involves some approximation and arbitrariness; however, the resulting error is negligible in view of the smallness of n_x^2 and $\tan^2 \Theta_{\parallel}$. We therefore propose the following simple rule: Replace n_x^2 with $\langle n_x^2 \rangle_{\text{aperture}}$ and $\tan^2 \Theta_{\parallel}$ with $\langle \tan^2 \Theta_{\parallel} \rangle_{\text{day}}$, as listed in Table 2-1, to obtain an effective contour error

$$\sigma_{\text{contour, effective}}^2 = \sigma_{\text{contour}_{\perp}}^2 + \langle n_x^2 \rangle_{\text{aperture}} \langle \tan^2 \Theta_{\parallel} \rangle \sigma_{\text{contour}_{\parallel}}^2 \quad (2-19)$$

The lack of perfect specularity of the reflector material [8] causes further beam spreading with an rms width σ_{specular} .

Table 2-1. QUANTITIES NEEDED FOR EVALUATION OF TRANSVERSE EFFECTS OF LONGITUDINAL CONTOUR ERRORS IN PARABOLIC TROUGH WITH EAST-WEST TRACKING AXIS

Average Over Aperture		Average Over Time of Day	
Rim Angle ϕ (degrees)	$\langle n_x^2 \rangle_{\text{aperture}} = 1 - \frac{\phi}{2 \tan(\phi/2)}$	Cutoff Time t_c (h)	$\langle \tan^2 \phi_{\parallel} \rangle_{\text{day}}$
0	0	0	0
30	0.023	3	0.2
45	0.052	4	0.5
60	0.093	5	0.9
75	0.147		
90	0.215		
105	0.297		
120	0.395		

Conceptually, concentrator alignment and tracking errors must be handled differently from mirror contour errors. Any given moment a concentrator is pointing in some direction, albeit with a transverse angular error $\Delta\theta_{\perp}$. It is only when an entire field of concentrators or a long time average is considered that a distribution in tracking error is obtained, described by a standard deviation σ_{tracking} . Similarly, errors resulting from displacement of the receiver can be characterized by an equivalent angular standard deviation $\sigma_{\text{displacement}}$ when averaged over a large collector field.

The total effective rms optical error σ_{optical} resulting from all of these effects is obtained by adding quadratically the individual standard deviations:

$$\begin{aligned} \sigma_{\text{optical}}^2 = & 4 \sigma_{\text{contour}_{\perp}}^2 + \sigma_{\text{specular}_{\perp}}^2 + \lambda(\phi) (4 \sigma_{\text{contour}_{\parallel}}^2 + \sigma_{\text{specular}_{\parallel}}^2) \\ & + \sigma_{\text{displacement}}^2 + \sigma_{\text{tracking}}^2, \end{aligned} \quad (2-20)$$

with

$$\lambda(\phi) = \langle n_x^2 \rangle_{\text{aperture}} \langle \tan^2 \theta_{\parallel} \rangle_{\text{day}}. \quad (2-21)$$

For collectors in which reflector and receiver do not move as a unit, the term σ_{tracking} must be multiplied by a factor of two; this is the case for Fresnel reflectors. Note also that the rule (Eq. 2-20) for adding standard deviations holds regardless of the detailed shape of the individual error distributions; in particular, they do not have to be Gaussian.

SECTION 3.0

CALCULATION OF FLUX AT RECEIVER

3.1 EFFECTIVE SOURCE

In a real solar concentrator, rays are incident from a range of directions, covering the solar disc and possibly the circumsolar region, and are reflected by an imperfect reflector surface that causes further angular dispersion. From the point of view of the receiver it does not matter whether the angular deviation of a ray from the design direction originates at the radiation source or at the reflector. This is illustrated in Figure 3-1. In Figure 3-1a a ray from a point source S strikes the reflector at a point R and would reach point Q of the receiver if the reflector were perfect. A real reflector differs from the design slope by an error θ_{slope} and thus the reflected ray reaches the receiver at Q', an angle $2\theta_{\text{slope}}$ away from Q. The same reflected ray would have resulted from a perfect reflector if the incident ray had come from S', an angle $2\theta_{\text{slope}}$ away from the point source S, as shown in Figure 3-1b. In general the distribution of the slope errors is nearly Gaussian, and the corresponding flux distribution at the receiver is indicated by the curves in Figures 3-1a and b.

The angular distribution of radiation from a real source like the sun is given by the functional dependence of brightness $B_{\text{source}}(\theta_{\text{in}})$ on incidence angle. Solar brightness data is usually reported as radial distribution $B_{\text{radial}}(\theta)$ in $W/m^2 \text{ sr}$, θ being measured from the center of the solar disc. For line focus systems it is convenient to transform the radial distribution to a linear one according to

$$B_{\text{linear}}(\theta_{\perp}) = \int_{-\infty}^{\infty} d\theta_{\parallel} B_{\text{radial}}(\theta), \quad \text{with } \theta = \sqrt{\theta_{\parallel}^2 + \theta_{\perp}^2} .$$

In the remainder of this paper only the linear brightness function (in $W/m^2 \text{ rad}$) is considered, and the subscripts for longitudinal and transverse are dropped.

If the mirror slope errors are characterized by a normalized distribution function $E(2\theta_{\text{slope}})$ in units of rad^{-1} , then the reflected intensity in the direction θ (measured from the design direction) is

$$dB(\theta, \theta_{\text{in}}) = E(\theta - \theta_{\text{in}}) B_{\text{source}}(\theta_{\text{in}}) d\theta_{\text{in}}, \tag{3-1}$$

where $(\theta - \theta_{\text{in}})/2 = \theta_{\text{slope}}$ is the slope error and $B_{\text{source}}(\theta_{\text{in}}) d\theta_{\text{in}}$ is the intensity of radiation coming from an angular region of width $d\theta_{\text{in}}$ around θ_{in} . Integrating over $d\theta_{\text{in}}$ produces the equivalent effective source:

$$B_{\text{eff}}(\theta) = \int_{-\infty}^{\infty} E(\theta - \theta_{\text{in}}) B_{\text{source}}(\theta_{\text{in}}) d\theta_{\text{in}} \tag{3-2}$$

The limits of integration can be extended to infinity because in practice the distribution will be negligible outside a range of a few degrees.

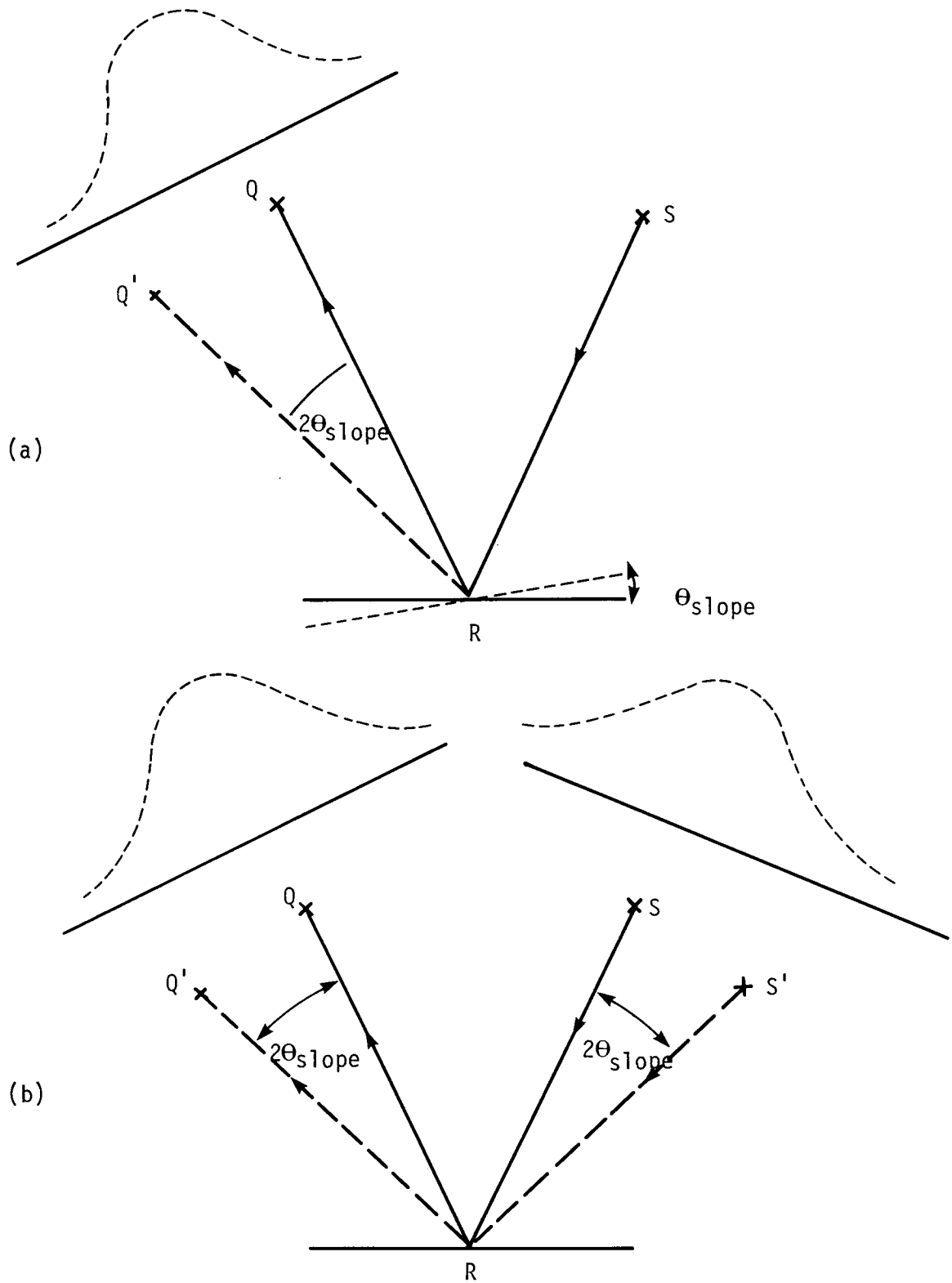


Figure 3-1. EQUIVALENCE BETWEEN (a) IMPERFECT REFLECTOR WITH POINT SOURCE AND (b) PERFECT REFLECTOR WITH SMEARED SOURCE.

In a real collector there will be several statistically independent sources of optical error: lack of perfect specularity [8], macroscopic surface deviations in position and slope, displacement of the receiver, and tracking errors. Averaged over time and over the entire collector or array of collectors, all of these errors can be assumed to be approximately Gaussian.* Even if the distributions for individual optical errors are not quite Gaussian, the central limit theorem of statistics [4] implies that the distribution resulting from their convolution can be expected to be nearly Gaussian (at least as long as the distribution is not dominated by a single non-Gaussian component). This is a most reasonable assumption; it is supported by the limited data which are available [9], and it is usually made in solar systems studies. The distribution function E of optical errors in Eq. 3-2 should, of course, include the convolution of all relevant optical errors.

Since the convolution of two Gaussians with zero mean and standard deviations σ_1 and σ_2 is again a Gaussian distribution, with standard deviation given by $\sigma^2 = \sigma_1^2 + \sigma_2^2$, sun and mirror errors can be replaced by an effective source

$$B_{\text{eff}}(\Theta) = \frac{1}{\sigma_{\text{optical}} \sqrt{2\pi}} \int_{-\infty}^{\infty} d\Theta' \exp\left(-\frac{\Theta'^2}{2\sigma_{\text{optical}}^2}\right) B_{\text{sun}}(\Theta - \Theta'). \quad (3-3)$$

The standard deviation σ_{optical} accounts for all optical errors and has been calculated in Eqs. 2-19, 2-20, and 2-21:

$$\begin{aligned} \sigma_{\text{optical}}^2 = & 4\sigma_{\text{contour, effective}}^2 + \sigma_{\text{specular, effective}}^2 + \sigma_{\text{displacement}}^2 \\ & + \sigma_{\text{tracking}}^2. \end{aligned} \quad (3-4)$$

For collectors in which the reflector and receiver do not move as a unit, σ_{tracking} must be multiplied by two.

In case the Gaussian model for the optical error is not acceptable, Eq. 3-3 must be replaced by the convolution of the appropriate error distribution functions. Certain reflector materials (for example, alzac) are characterized by the sum of two Gaussian distributions of relative weights R_1 and R_2 and widths $\sigma_{\text{specular } 1}$ and $\sigma_{\text{specular } 2}$. This type of material (which does not appear to be very practical for focusing solar collectors) can be dealt with by replacing the single Gaussian distribution in Eq. 3-3 with a sum of two Gaussian distributions with weights R_1 and R_2 and widths $\sigma_{\text{optical } 1}$ and $\sigma_{\text{optical } 2}$ (corresponding to each of the two nonspecular components) [8,9].

*Tracking errors may differ from this model when the tracking system has a significant tolerance band; for this case, a flat top with sloping shoulders may be more appropriate.

3.2 ANGULAR ACCEPTANCE FUNCTION

In the framework of this paper, aberrations due to off-axis incidence on a perfect reflector are not included among errors but are accounted for by means of the angular acceptance function.

The angular acceptance function $f(\Theta)$ is defined as the fraction of rays incident on the collector aperture at an angle Θ (from the optical axis) which reaches the receiver. This function depends on the configuration of reflector and receiver. For example, an untruncated compound parabolic concentrator (CPC) [7] of acceptance half angle Θ_a is characterized by the angular acceptance function

$$f_{\text{CPC}}(\Theta) = \begin{cases} 1 & \text{for } |\Theta| < \Theta_a \\ 0 & \text{for } |\Theta| > \Theta_a \end{cases}; \quad (3-5)$$

in other words, all rays within Θ_a are accepted, all rays outside are rejected.

For a parabolic trough of rim angle Φ with cylindrical receiver, the angular acceptance function is more complicated and can be calculated from the geometric relations in Fig. 3-2a. The focal length is f ; the aperture width, D ; and the receiver tube diameter, d . The geometric concentration C is

$$C = \frac{D}{\pi d} . \quad (3-6)$$

Light rays incident at point $P = (x, y)$ of the reflector hit the receiver, provided their angle of incidence Θ (measured from the optical axis) satisfies

$$|\Theta| < \Theta_x, \quad \text{with } \sin \Theta_x = \frac{d/2}{\sqrt{x^2 + (f - y)^2}} = \frac{d}{2f \left[1 + \left(\frac{x}{2f} \right)^2 \right]}. \quad (3-7)$$

$|\Theta| = \Theta_x$ is the angle at which they reach the receiver tube tangentially. Θ_x decreases with x . Therefore, with $x = D/2$, Eq. 3-7 yields the largest angle Θ_1 for which all incident rays are accepted. This angle Θ_1 , which has sometimes been called the acceptance half angle of a parabolic trough [7], can be written in terms of rim angle and concentration as

$$\sin \Theta_1 = \frac{\sin \Phi}{\pi C} . \quad (3-8)$$

For the angular acceptance function this implies that $f_{\text{PT,cyl}}(\Theta) = 1$ for $|\Theta| < \Theta_1$. For incidence angles larger than Θ_1 but smaller than Θ_2 , given by

$$\sin \Theta_2 \approx \frac{d}{2f} , \quad (3-9)$$

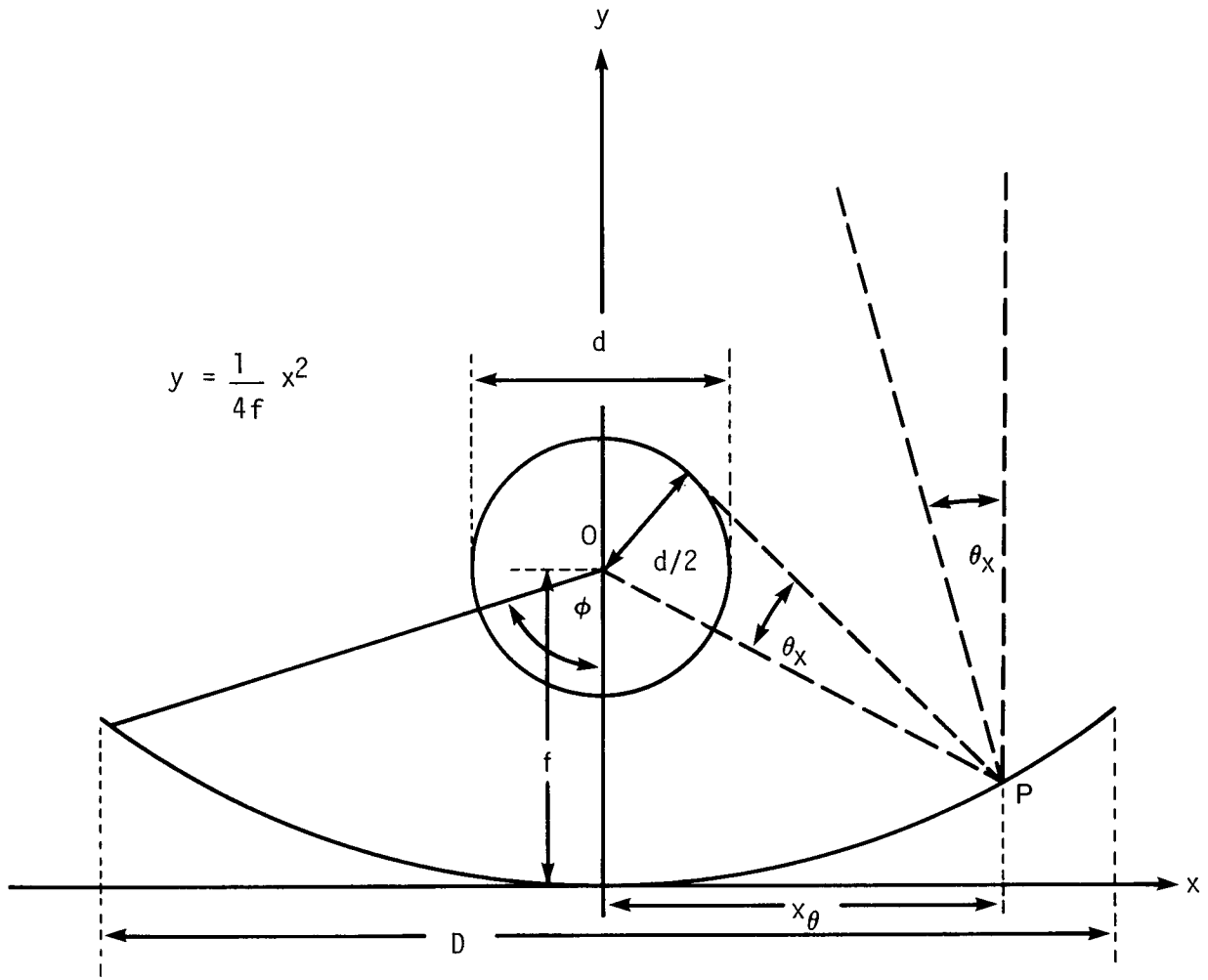


Figure 3-2a. GEOMETRIC RELATIONS FOR THE CALCULATION OF THE ANGULAR ACCEPTANCE FUNCTION.

only the central section of the aperture is effective, from $-x_{\Theta}$ to x_{Θ} , with

$$x_{\Theta} = 2f \left(\frac{d}{2f \sin \Theta} - 1 \right)^{1/2}, \quad (3-10)$$

and the angular acceptance equals $2x_{\Theta}/D$. For angles larger than Θ_2 only direct hits are accepted, but this region will not be of interest in this paper. It is convenient to express everything in terms of rim angle and concentration by means of the relation

$$\frac{D}{4f} = \tan \frac{\Phi}{2}. \quad (3-11)$$

Neglecting complications or inaccuracies that may arise for very low concentrations, very large incidence angles, or very small rim angles (cases which are not of interest for solar energy applications), the angular acceptance function for the parabolic trough with cylindrical receiver, rim angle Φ , and concentration C can be summarized as*

$$f_{\text{PT,cylindrical}}(\Theta) = \begin{cases} 1 & \text{for } |\Theta| < \Theta_1 \\ \cot \frac{\Phi}{2} \left(\frac{2 \tan(\Phi/2)}{\pi C \Theta} - 1 \right)^{1/2} & \text{for } \Theta_1 < |\Theta| < \Theta_2 \\ 0 & \text{for } |\Theta| > \Theta_2 \end{cases} \quad (3-12)$$

with

$$\Theta_1 = \frac{\sin \Phi}{\pi C} = \Theta_2 \cos^2(\Phi/2) \quad (3-8)$$

and

$$\Theta_2 = \frac{2 \tan(\Phi/2)}{\pi C}. \quad (3-13)$$

C is assumed large enough ($C \gtrsim 3$) to justify replacing $\sin \Theta$ with Θ for $|\Theta| \lesssim \Theta_2$.

For the parabolic trough with a flat one-sided receiver, the angular acceptance function can be derived in a similar manner. The result is

*The addition of a glass tube, placed concentrically around a tubular receiver, has no effect on the angular acceptance function [10].

$$f_{PT,flat-one-sided}(\theta) = \begin{cases} 1 & \text{for } |\theta| < \theta_1 = \frac{\sin \phi \cos \phi}{C} \\ \cot \frac{\phi}{2} \left\{ \left[\left(4 + \frac{\tan(\phi/2)}{\theta C} \right) \frac{\tan(\phi/2)}{\theta C} \right]^{1/2} - 1 - \frac{\tan(\phi/2)}{\theta C} \right\}^{1/2} & \text{for } \theta_1 < |\theta| < \theta_2 = \frac{2}{C} \tan \frac{\phi}{2} \\ 0 & \text{for } |\theta| > \theta_2 . \end{cases} \quad (3-14)$$

This function is unaffected by the addition of a CPC second-stage concentrator of acceptance half angle ϕ because such a CPC only prevents rays with $|\theta| > \theta_2$ from reaching the receiver.

For future reference we note that the angular acceptance function depends only on the product $C\theta$, not on C and θ separately. The angular acceptance functions are plotted schematically in Figs. 3-2b and c for the cylindrical and flat receivers.

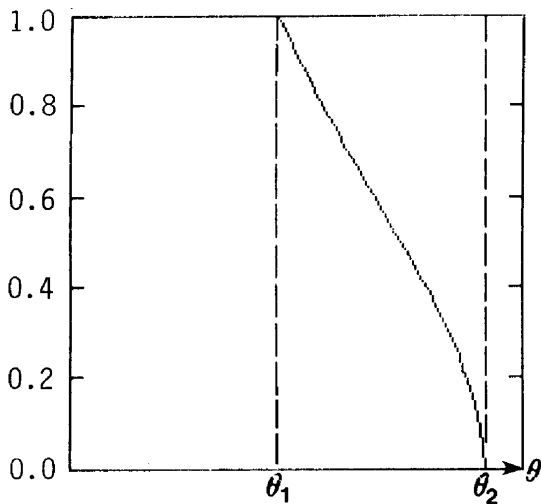


Figure 3-2b. ANGULAR ACCEPTANCE FUNCTION FOR $\phi = 90^\circ$ TROUGH WITH CYLINDRICAL RECEIVER (SCHEMATIC).

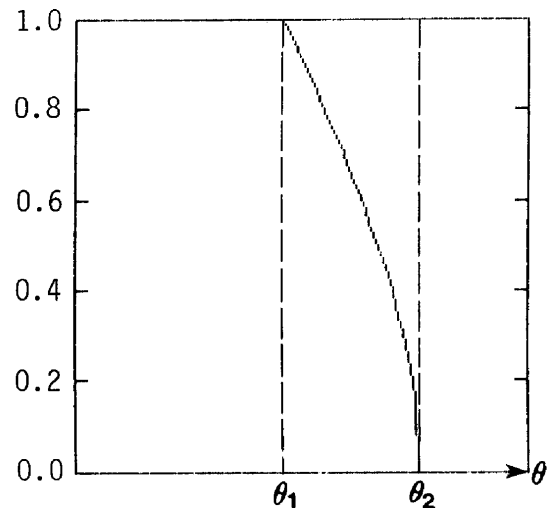


Figure 3-2c. ANGULAR ACCEPTANCE FUNCTION FOR $\phi = 45^\circ$ TROUGH WITH FLAT RECEIVER (SCHEMATIC).

3.3 FLUX AT RECEIVER AND INTERCEPT FACTOR

The effective source function $B_{\text{eff}}(\Theta)$ of Eq. 3-3 gives the intensity of radiation ($\text{W}/\text{m}^2 \text{ rad}$) coming from the direction Θ ; it accounts correctly for the shape of the sun and for all optical errors. The angular acceptance function $f(\Theta)$ states how much of this radiation is transmitted to the receiver.* The total flux intercepted by the receiver is obtained by multiplying these two functions and integrating over all incidence angles:

$$q_{\text{in}} = \int_{-\infty}^{\infty} d\Theta f(\Theta) B_{\text{eff}}(\Theta). \quad (3-15)$$

The receiver size enters through the concentration ratio C in the angular acceptance function.

Dividing Eq. 3-15 by the total incident flux

$$I_b = \int_{-\infty}^{\infty} d\Theta B_{\text{eff}}(\Theta), \quad (3-16)$$

one obtains the intercept factor

$$\gamma = \int_{-\infty}^{\infty} d\Theta f(\Theta) B_{\text{eff}}(\Theta)/I_b, \quad (3-17)$$

which is useful because it is independent of the intensity.

This formulation is equivalent to a detailed computer ray-trace program. It is much simpler and faster, requiring at most a double integration. (A further integration may be needed to convolute non-Gaussian optical errors.) The relevant parameters and their interrelation are clearly identified. In many cases approximations can be made to the point where the explicit result can be presented in graphical form. This is discussed in the following section.

Time-of-day effects can be treated exactly by evaluating q_{in} of Eq. 3-15 for each hour of the day using the projected sun shape discussed in Section 2.0. In most cases, however, a single calculation with an effective average sun shape for the whole day (see Section 2.2) is sufficiently accurate.

* $f(\Theta)$ is defined as a purely geometrical quantity. Absorption losses will be accounted for later by a multiplicative factor, the transmittance-reflectance-absorptance product ($\rho \tau \alpha$).

For collectors with cylindrical receivers the derivative of γ with respect to concentration C can be used to calculate the distribution of incidence angles on the receiver. Consider the radiation intercepted by a virtual receiver, smaller than the real receiver and corresponding to a concentration \tilde{C} , placed inside the real receiver which has concentration C . One can show that there is a one-to-one relationship,

$$\cos \beta = \sqrt{1 - C^2/\tilde{C}^2} \cos \Theta , \tag{3-18}$$

between the incidence angle β of a ray on the actual receiver surface and the concentration $\tilde{C} < C$ of the virtual receiver which the same ray would hit tangentially; Θ is the incidence angle of the ray on the collector aperture. From this it follows that the unnormalized probability distribution of incidence angles β on the receiver surface is given by

$$\Gamma(\beta, \Theta) = - \frac{\tilde{C}^3}{C_o^2} \frac{\sin \beta \cos \beta}{\cos^2 \Theta} \frac{d\gamma(\tilde{C})}{d\tilde{C}} . \tag{3-19}$$

This point is of interest because the absorptance of most surfaces decreases at large incidence angles. For example, if the absorptance α of a flat surface is given as a function $\alpha(\beta)$ of incidence angle β , then the effective absorptance of this surface, when used on a cylindrical absorber tube, is

$$\alpha_{\text{eff}} = \frac{\int_0^{\pi/2} d\beta \alpha(\beta) \Gamma(\beta, \Theta)}{\int_0^{\pi/2} d\beta \Gamma(\beta, \Theta)} , \tag{3-20}$$

where Θ is the angle of incidence on the collector aperture.

For collectors with flat receivers the derivative of γ with respect to C yields the spatial flux distribution on the receiver. The incidence angle distribution can be obtained from the derivative of γ with respect to rim angle Φ .

Thus far tracking errors have been assumed to be averaged over time, since the collector is, on an average, aligned correctly. The effect of misalignment on the instantaneous efficiency can also be calculated. If the optical axis of the collector points an angle Θ_{\perp} away from the design direction (center of the source), the origin of the angular acceptance function is shifted by Θ_{\perp} and the intercept factor is given by a straightforward modification of Eq. 3-17:

$$\gamma(\Theta_{\perp}) = \int_{-\infty}^{\infty} d\theta' f(\theta' - \Theta_{\perp}) B_{\text{eff}}(\theta')/I_b . \tag{3-21}$$

SERIO 

SECTION 4.0

APPROXIMATION OF SUN SHAPE BY GAUSSIAN DISTRIBUTION

When the optical errors are large compared to the width of the sun, Eq. 3-3 is insensitive to details of the sun shape. In this case it is convenient to approximate the sun shape by a Gaussian distribution:

$$B_{\text{sun,Gauss}}(\Theta) = \frac{I_b}{\sigma_{\text{sun}} \sqrt{2\pi}} \exp \left[-\frac{\Theta^2}{2\sigma_{\text{sun}}^2} \right] \quad (4-1)$$

with the variance

$$\sigma_{\text{sun}}^2 = \frac{\int_{-\infty}^{\infty} d\Theta \Theta^2 B_{\text{sun,real}}(\Theta)}{\int_{-\infty}^{\infty} d\Theta B_{\text{sun,real}}(\Theta)} \quad (4-2)$$

of the real sun. (Note that σ_{linear} and σ_{radial} for linear and radial brightness distributions are related by $\sigma_{\text{linear}} = \sigma_{\text{radial}}/\sqrt{2}$. In this sense the sun appears to be narrower for a line focus collector than for a point focus collector.)

The resulting effective source is also a Gaussian distribution:

$$B_{\text{eff,Gauss}}(\Theta) = \frac{I_b}{\sigma_{\text{tot}} \sqrt{2\pi}} \exp \left(-\frac{\Theta^2}{2\sigma_{\text{tot}}^2} \right) \quad (4-3)$$

with width

$$\sigma_{\text{tot}} = \left(\sigma_{\text{optical}}^2 + \sigma_{\text{sun}}^2 \right)^{1/2}. \quad (4-4)$$

The intercept factor γ is defined as the ratio of the flux reaching the receiver over the incident beam irradiance I_b :

$$\gamma_{\text{Gauss}} = \int_{-\infty}^{\infty} d\Theta f(C\Theta) \frac{1}{\sigma_{\text{tot}} \sqrt{2\pi}} \exp \left(-\frac{\Theta^2}{2\sigma_{\text{tot}}^2} \right). \quad (4-5)$$

Since the angular acceptance is a function of $C\Theta$ only, γ_{Gauss} depends only on the product $\sigma_{\text{tot}} C$, not on C and σ_{tot} separately. For the parabolic trough the resulting integrals do not seem to be expressible in closed form; γ_{Gauss} has been evaluated numerically and plotted versus $\sigma_{\text{tot}} C$ for several values of rim angle, for the cylindrical receiver in Figure 4-1a and for the flat one-sided receiver in Figure 4-1b.

To evaluate the error introduced by using the Gaussian sun instead of the real sun, the intercept factor γ is compared in Figure 4-2a through c as calculated with the measured

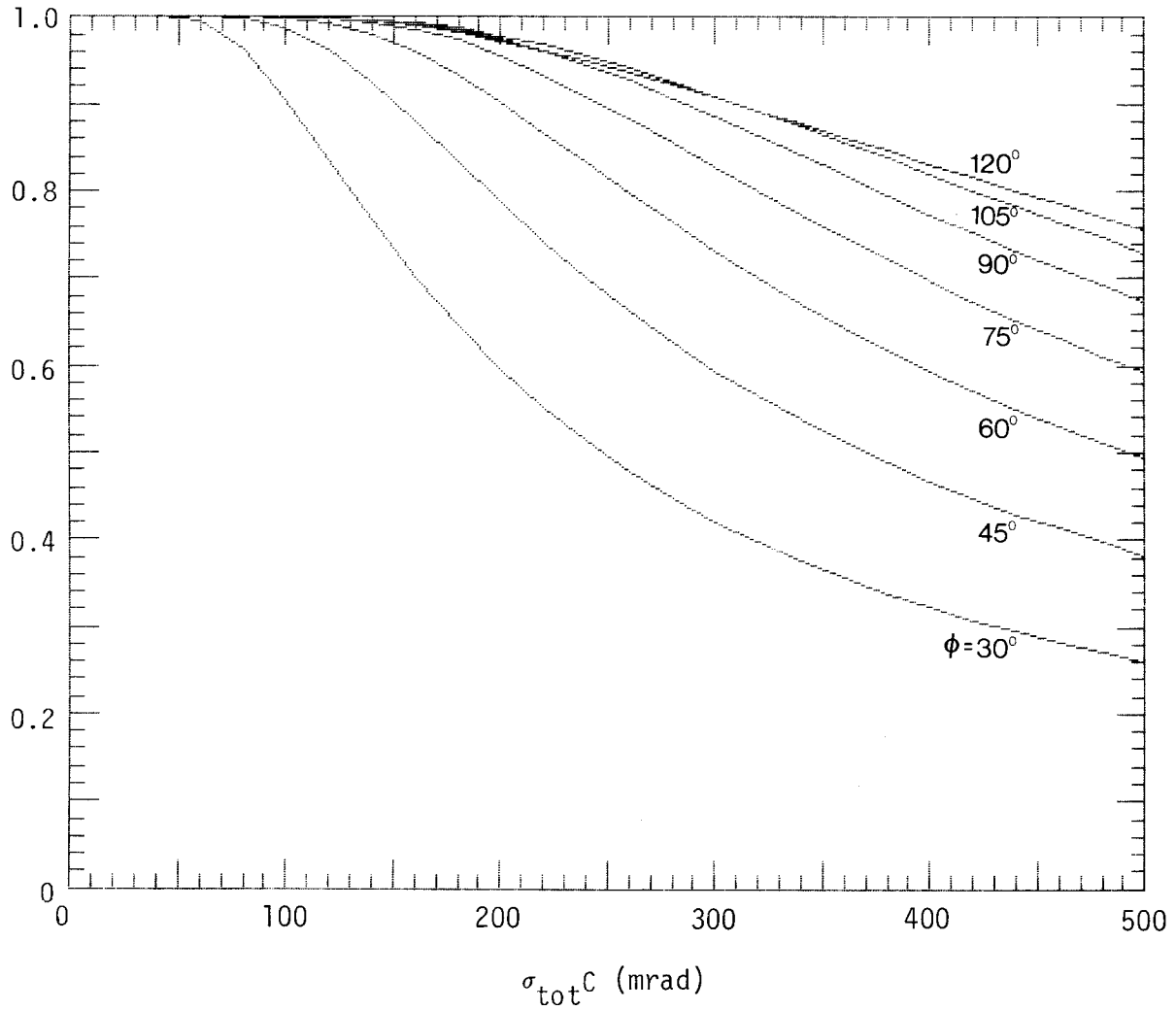


Figure 4-1a. INTERCEPT FACTOR γ VERSUS $\sigma_{TOT}C$ FOR DIFFERENT RIM ANGLES ϕ FOR A CYLINDRICAL RECEIVER (GAUSSIAN APPROXIMATION).

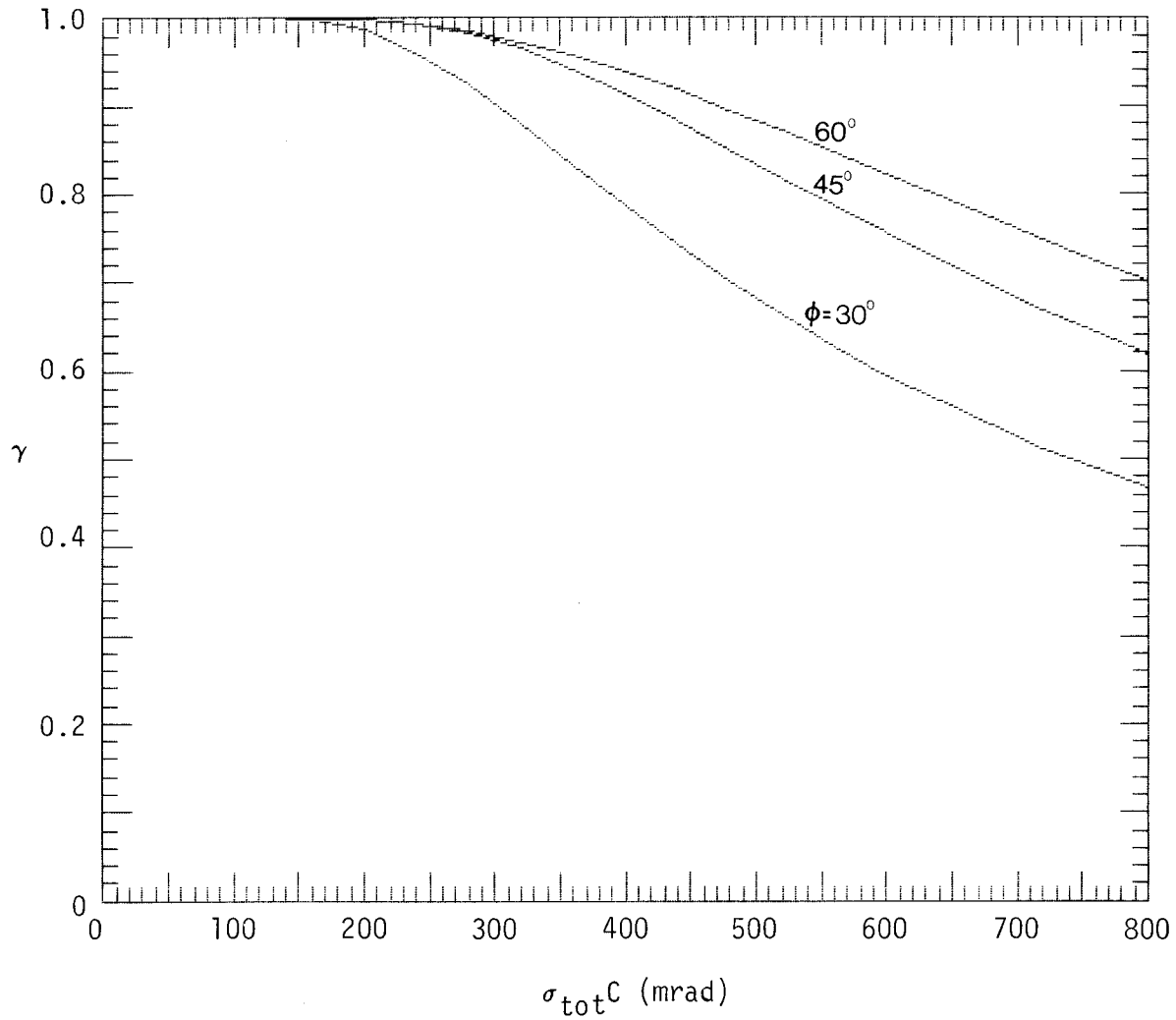


Figure 4-1b. INTERCEPT FACTOR γ VERSUS $\sigma_{TOT}C$ FOR DIFFERENT RIM ANGLES ϕ FOR A FLAT RECEIVER (GAUSSIAN APPROXIMATION).

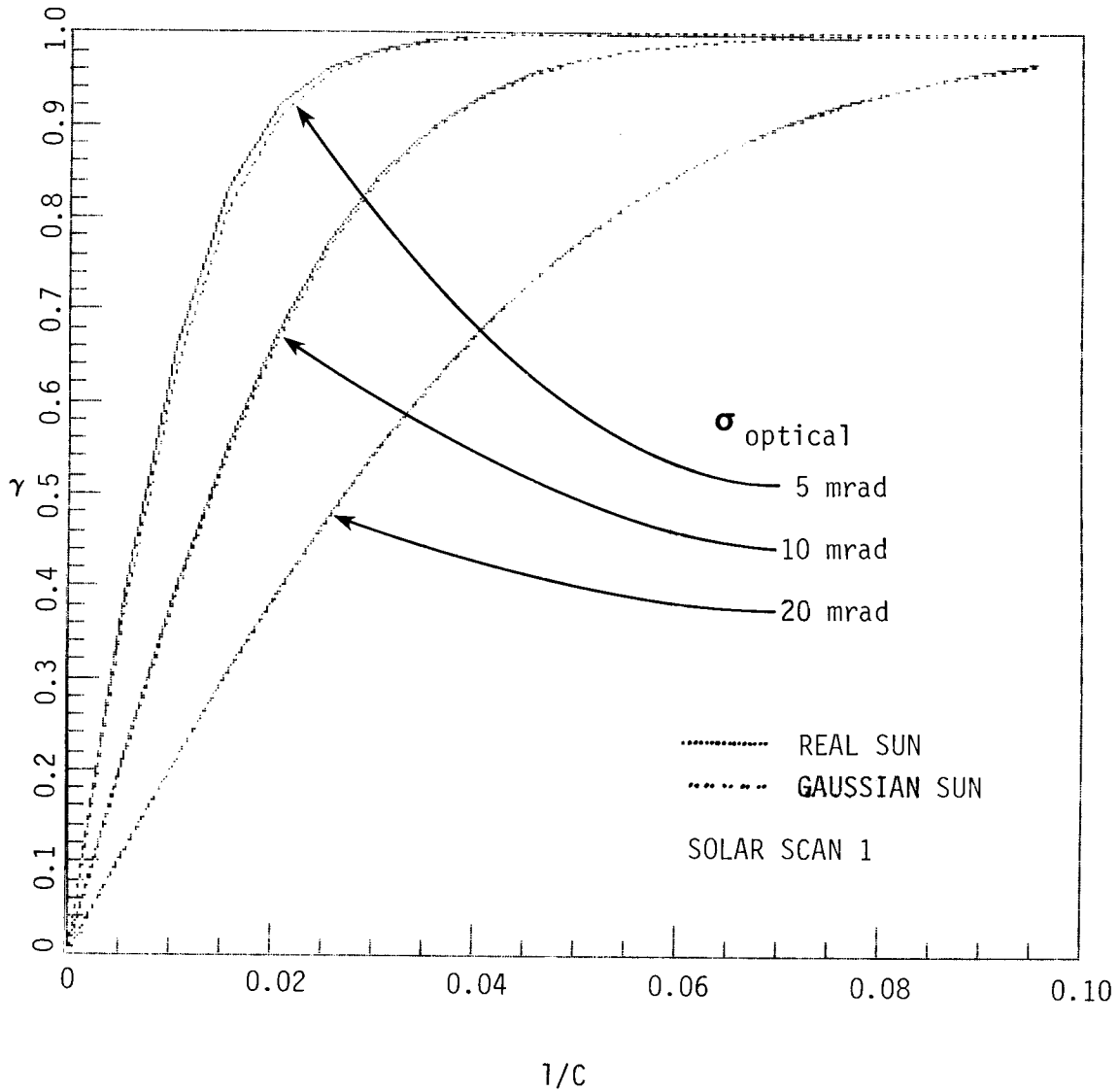


Figure 4-2a. INTERCEPT FACTOR γ VERSUS $1/C$ FOR CIRCUMSOLAR SCAN NUMBER 1 (NARROW).

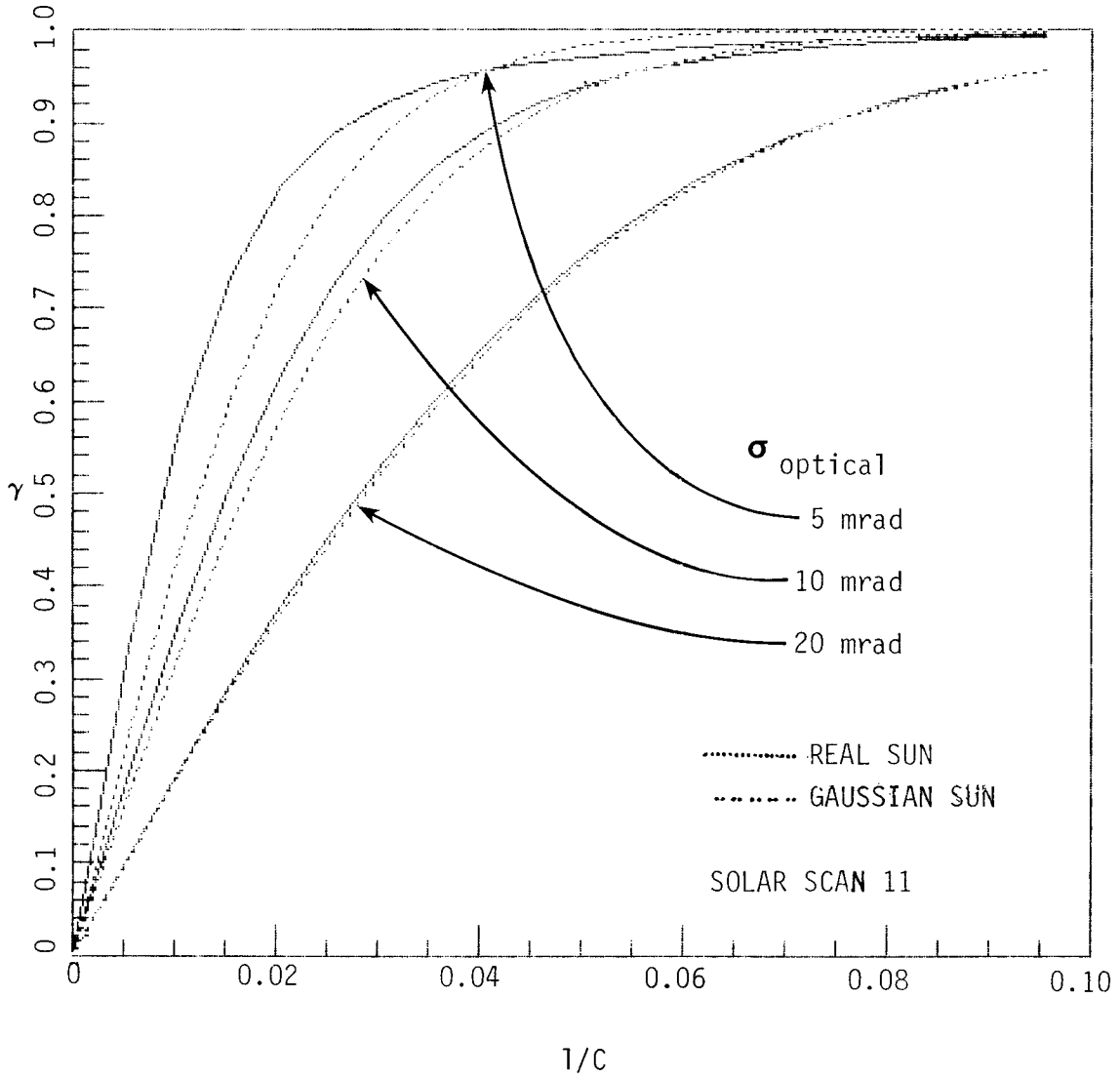


Figure 4-2b. INTERCEPT FACTOR γ VERSUS $1/C$ FOR CIRCUMSOLAR SCAN NUMBER 11 (WIDE).

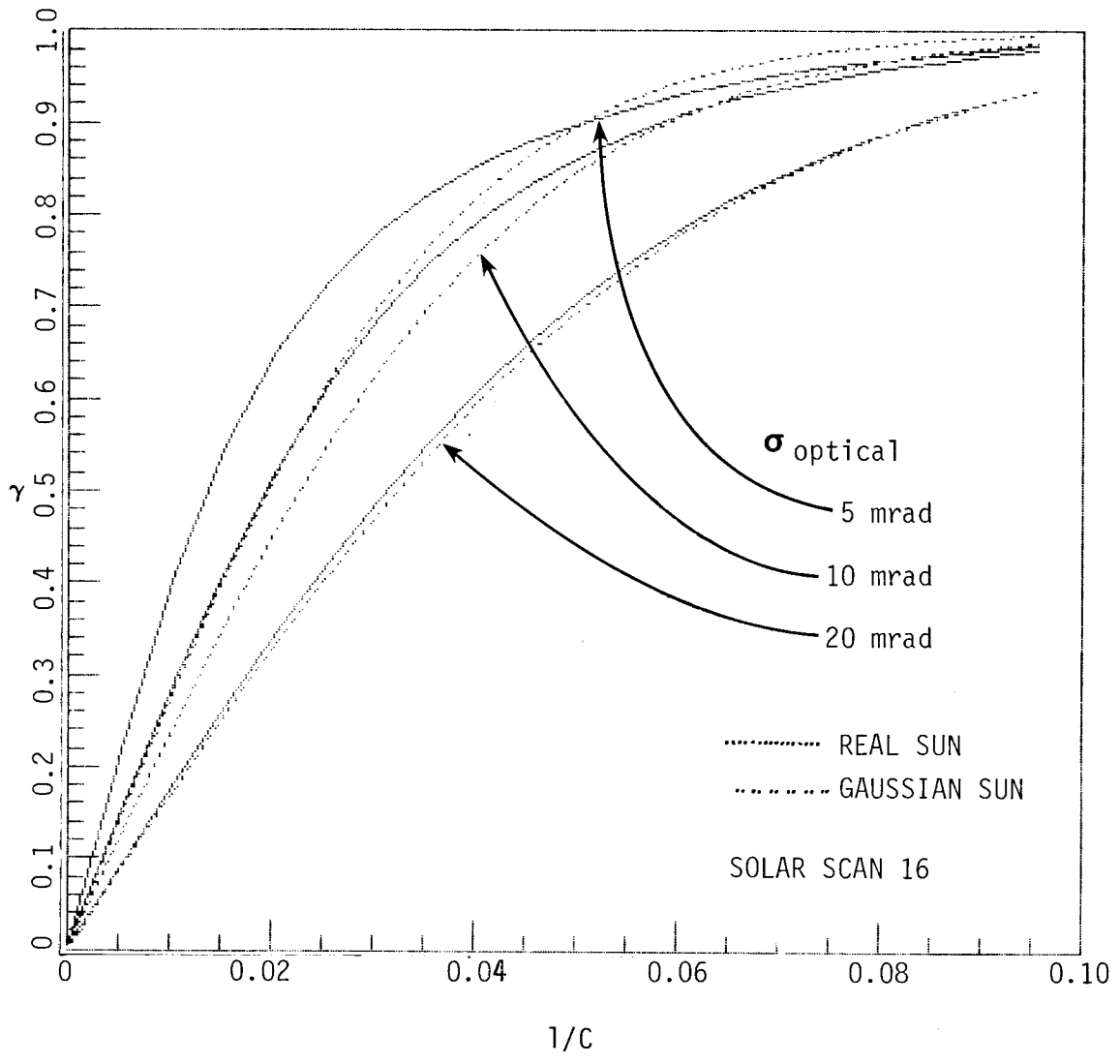


Figure 4-2c. INTERCEPT FACTOR γ VERSUS $1/C$ FOR CIRCUMSOLAR SCAN NUMBER 16 (VERY WIDE).

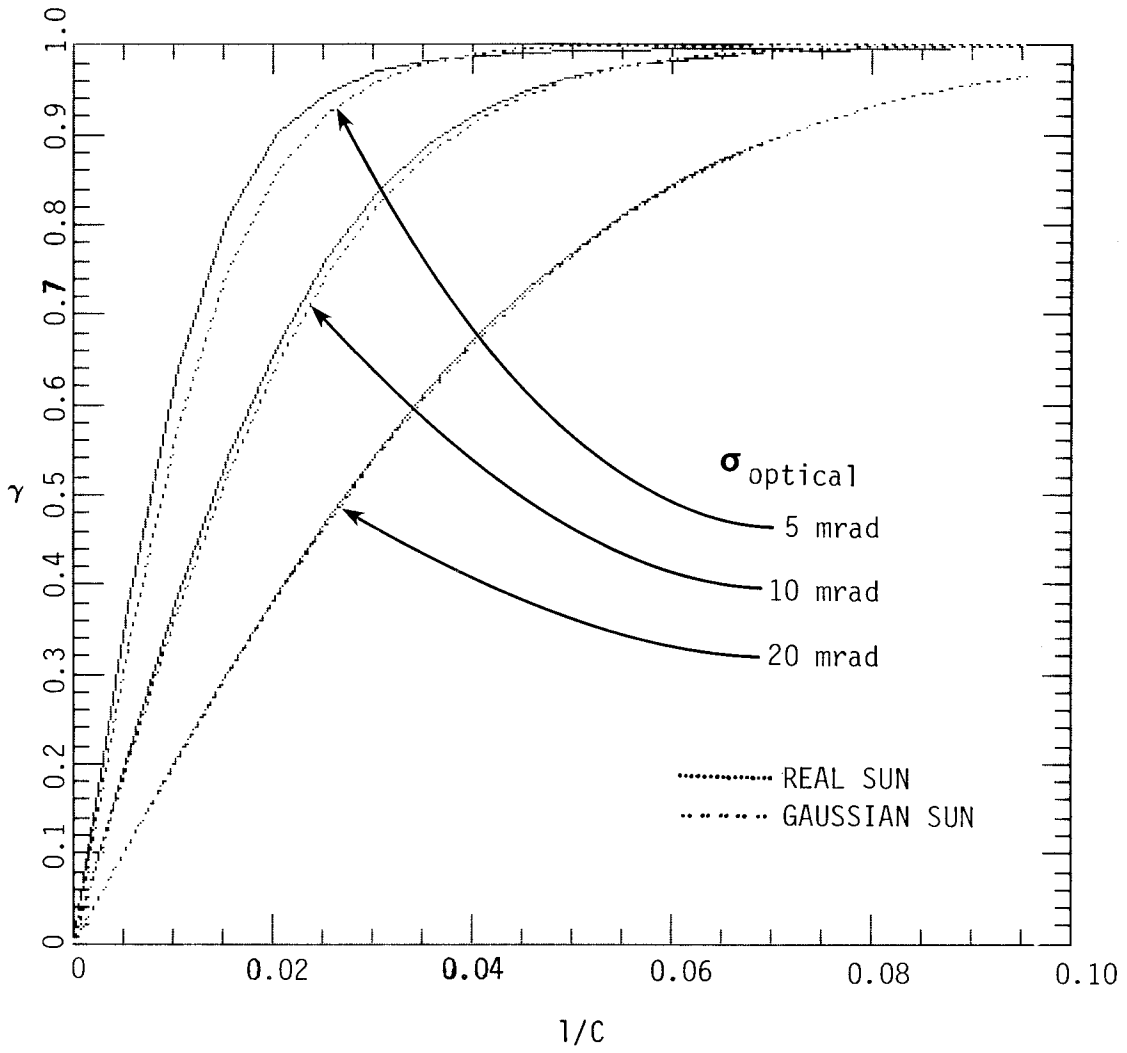


Figure 4-2d. AVERAGE OF INTERCEPT FACTOR γ VERSUS $1/C$ OVER CIRCUMSOLAR SCANS 1 THROUGH 10.

solar profile (solid line) and as calculated with the corresponding Gaussian shape (dotted line). A cylindrical receiver and 90° rim angle have been assumed. Curves are shown for three error sizes, $\sigma_{\text{optical}} = 5, 10, \text{ and } 20$ mrad, and for three solar profiles, corresponding to clear sky, haze, and heavy haze. These profiles are numbers 1, 11, and 16 of the standard circumsolar profiles provided by the Lawrence Berkeley Laboratory [5]. The insolation values and rms widths for the 16 profiles are listed in Table 4-1. The broad sun shapes seem to be associated only with times when the beam component is so low ($I_b \leq 500 \text{ W/m}^2$) that little energy can be collected; thus only the narrow and medium shapes need to be considered [11]. This suggests the use of an average intercept factor for all circumsolar scans with high insolation. The unweighted average over scans one through ten ($I_b > 500 \text{ W/m}^2$) is plotted in Figure 4-2d, with the same notation as in Figures 4-2a through c. The Gaussian sun shape (dashed line in Figure 4-2d) is based on the standard deviation

$$\sigma_{\text{sun,average}} = 4.1 \text{ mrad}, \quad (4-6)$$

which is the average of the standard deviations for scans one through ten. As for optical errors, current plans [12] for advanced parabolic trough collectors suitable for mass production call for a value of σ_{optical} around 7 mrad. Whether greater optical accuracy is compatible with the low cost requirements of solar applications remains uncertain.

Figures 4-2 a-d show that the Gaussian sun approximation is excellent for optical errors beyond 20 mrad, regardless of sun shape. For narrow sun shapes the approximation is good to 1%, even for the rather small optical error of 5 mrad. More detailed analysis seems to be necessary for the case of intermediate solar widths and very good optical quality $\sigma_{\text{optical}} < 5$ mrad.

In any case it is worth noting that the Gaussian approximation consistently underestimates the radiation reaching the receiver for any practical value of C . Usually C will be chosen such that on a clear day approximately 95% of the incident rays reach the receiver; i.e., losses due to spillover amount to about 5%. (The Gaussian approximation would overestimate the collected flux only if the concentration ratio were much smaller than this value.) Therefore, a simple upper bound on the loss of performance due to circumsolar radiation is obtained by considering the change in σ_{tot} caused by an increase in σ_{sun} . This is illustrated by the examples in Section 6. Furthermore, the Gaussian approximation is useful for determining the optimal concentration ratio, as shown in Section 5.0.

Table 4-1. PARAMETERS FOR THE 16 STANDARD LBL CIRCUMSOLAR SCANS

Data Set	Date	Solar Times (h)	Location	I_{disk} (4.80 mrad) (W/m ²)	I_b (pyrheliometer) (W/m ²)	Circumsolar Ratio	σ_{sun} Linear Geometry (mrad)
1	Aug. 7 1976	11.72	Albuquerque	947.8	954	0.0082	2.7
2	Aug. 25 1976	9.36	Fort Hood	708.9	715	0.0100	2.7
3	Nov. 20 1976	11.22	Fort Hood	894.8	918	0.0270	2.5
4	Nov. 22 1976	14.89	Fort Hood	775.8	795	0.0290	3.5
5	Dec. 14 1976	11.29	Albuquerque	919.5	949	0.0345	3.2
6	Dec. 29 1976	15.45	Fort Hood	714.9	748	0.0571	4.9
7	Jan. 25 1977	9.34	Albuquerque	736.6	802	0.0888	4.2
8	Dec. 29 1976	14.00	Fort Hood	705.4	782	0.1061	4.3
9	Dec. 14 1976	12.92	Albuquerque	699.8	802	0.1461	6.1
10	Jan. 25 1977	10.79	Albuquerque	517.3	639	0.2042	5.7
11	Dec. 14 1976	10.21	Albuquerque	340.6	469	0.2938	7.2
12	Dec. 29 1976	13.64	Fort Hood	217.5	348	0.3990	8.1
13	Jan. 25 1977	9.88	Albuquerque	164.0	292	0.4708	10.0
14	Dec. 29 1976	10.39	Fort Hood	168.1	299	0.5260	15.0
15	Dec. 29 1976	12.74	Fort Hood	40.5	87	0.5870	13.0
16	Jan. 25 1977	12.78	Albuquerque	29.5	86	0.6920	13.0



SECTION 5.0

OPTIMAL CONCENTRATION RATIO

Concentration entails necessarily the loss of some diffuse and possibly the loss of some circumsolar radiation. If maximization of absorbed energy were the goal, $C = 1$ would be chosen; however, in thermal collectors heat losses increase with receiver size and therefore the optimal concentration ratio, the one maximizing delivered energy, will be greater than one. In this section a formula is derived for determining the optimal concentration ratio.*

Heat losses can be assumed to scale as $1/C$:

$$q_{\text{loss}} = \frac{q_L}{C} . \quad (5-1)$$

This statement is exact if the aperture area is varied while the receiver size is kept fixed. If the aperture is held constant, variation of receiver size may cause slight deviations from the scaling rule (Eq. 5-1) because convective heat transfer may depend weakly on absolute size. For the derivation of a general procedure for finding the optimal concentration ratio, the scaling rule is the most reasonable choice.

In line focus collectors two additional effects should be considered: the collection of diffuse sky radiation, and the shading of the aperture by the receiver. Typical levels of diffuse radiation I_d range from 100 to 200 W/m^2 , and a fraction $1/C$ of this is collected [7]:**

$$q_{\text{diffuse}} = \frac{I_d}{C} . \quad (5-2)$$

For example, with $C = 25$, diffuse radiation amounts to 4 to 8 W/m^2 , which is small compared to typical heat losses q_{loss} on the order of 100 W/m^2 , but it is not negligible. Shading also scales with C ; the portion of the beam irradiance I_b which is prevented from reaching the receiver because of shading can be written as

*Similar considerations apply to photovoltaic concentrators where, per unit area, receiver cost is much higher than reflector cost. Here the optimal concentration ratio minimizes cost for delivered energy.

**Since diffuse radiation is collected along the length of the receiver, this formula is quite insensitive to anisotropy of sky radiation.

$$q_{\text{shading}} = \frac{X_S}{C} I_b, \quad (5-3)$$

where X_S depends on the geometry.

An example is a parabolic trough with an aperture width of $D = 200$ cm and a cylindrical receiver of $d = 2.5$ cm diameter, surrounded by a glass envelope of $d_{\text{glass}} = 5$ cm outer diameter* for which

$$X_S = \frac{d_{\text{glass}} - d}{\pi d} = 0.318$$

$$C = \frac{D}{\pi d} = 25, \text{ and}$$

$$q_{\text{shading}} = 11.25 \text{ W/m}^2 \text{ if } I_b = 900 \text{ W/m}^2.$$

The design goal is to maximize the net flux collected by the receiver:

$$\begin{aligned} q_{\text{net}} &= (\rho \tau \alpha) (q_{\text{diffuse}} - q_{\text{shading}} + q_{\text{in}}) - q_{\text{loss}} \\ &= (\rho \tau \alpha) \left[\frac{I_d}{C} - \frac{X_S I_b}{C} + \int_{-\infty}^{\infty} d\theta f(\theta) B_{\text{eff}}(\theta) \right] - \frac{q_L}{C}. \end{aligned} \quad (5-4)$$

The factor $(\rho \tau \alpha)$ accounts for the effective transmittance and absorptance of the collector, and f and B_{eff} are the angular acceptance (Eq. 3-12) and effective source (Eq. 3-3), respectively. $(\rho \tau \alpha)$, I_d , X_S , and q_L enter only in the combination

$$X = X_S + \left(\frac{q_L}{(\rho \tau \alpha)} - I_d \right) / I_b, \quad (5-5)$$

which shall be referred to as critical intensity ratio.

The optimal concentration ratio C_o is then found by setting the derivative of q_{net} with respect to C equal to zero:

$$\left. \frac{dq_{\text{net}}}{dC} \right|_{C = C_o} = 0. \quad (5-6)$$

*Rays passing through the glass but missing the receiver on their first pass deviate so much from the correct direction as to miss the receiver altogether.

Even though for small values of σ_{optical} the Gaussian approximation for the sun may result in significant underprediction for the absorbed flux, it may be acceptable for finding C_o because the net power q_{net} , being near its maximum, is a slowly varying function of C . The Gaussian approximation is attractive because C_o depends only on $(\sigma_{\text{tot}} C)$ and X and can therefore be obtained from a single graph. To test the validity of this assumption, the exact value $C_{o,\text{exact}}$ is determined for a wide range of parameters for a real sun and the corresponding $C_{o,\text{Gauss}}$ for a Gaussian sun. The net power q_{net} (for the real circumsolar profile) is then calculated for these two concentration values and the results are compared. The discrepancy*

$$\frac{q_{\text{net}}(\text{real}, C_{o,\text{real}}) - q_{\text{net}}(\text{real}, C_{o,\text{Gauss}})}{q_{\text{net}}(\text{real}, C_{o,\text{real}})} \quad (5-7)$$

is shown in Table 5-1 for $\sigma_{\text{optical}} = 5, 10, 20$ mrad; $q_L = 1000, 2000, \dots, 8000$ W per m^2 of receiver surface; and three solar shapes (narrow, scan No. 1; wide, scan No. 11; very wide, scan No. 16).

Table 5-1 shows not only the closeness of the approximation for C_o provided by the Gaussian sun shape, but also how much C_o varies with sun shape. For narrow sun shapes $C_{o,\text{Gauss}}$ approximates $C_{o,\text{real}}$ within 4%, even for small optical errors; and the change in q_{net} associated with such a change in C_o is less than a tenth of a percent and negligible. Even for wide sun shapes the difference in q_{net} optimized for the real sun and for the Gaussian sun is only a few percent.** The very wide sun shape has such a low insolation level that the collectible energy is negligible, and for large σ or high heat loss no energy can be collected at all. More important is the fact that the difference between $C_{o,\text{real}}$ and $C_{o,\text{Gauss}}$ for the narrow sun shape is of the same order of magnitude as the change in C_o between different sun shapes. Furthermore, the accuracy of a determination of C_o is limited by the uncertainty of σ_{optical} , typically on the order of 10%. Therefore, $C_{o,\text{Gauss}}$, as obtained by the Gaussian approximation for the narrow sun shape, provides an excellent compromise for the optimal concentration value under all reasonable operating conditions.

For a Gaussian sun of total flux I_b (in W/m^2), the effective source is

$$B_{\text{eff,Gauss}}(\theta) = \frac{I_b}{\sigma_{\text{tot}} \sqrt{2\pi}} \exp\left(-\frac{\theta^2}{2 \sigma_{\text{tot}}^2}\right). \quad (5-8)$$

*In this comparison we have set $X_S = 0 = I_d$ and $(\rho \tau \alpha) = 1$ because their precise values do not matter.

**In going from a narrow to a wide sun shape, C_o can either increase or decrease; this depends on the relative importance of reducing q_{loss} or enhancing γ .

TABLE 5-1. OPTIMIZATION OF CONCENTRATION RATIO FOR REAL SUN AND FOR GAUSSIAN SUN^a

σ_{optical} (mrad)	Scan #1 (narrow) $I_b = 954 \text{ W/m}^2; \sigma_{\text{sun}} = 2.7 \text{ mrad}$						Scan #11 (Wide) $I_b = 469 \text{ W/m}^2; \sigma_{\text{sun}} = 7.2 \text{ mrad}$						Scan #16 (Very Wide) $I_b = 86 \text{ W/m}^2; \sigma_{\text{sun}} = 13.0 \text{ mrad}$																																					
	5	10	20	5	10	20	5	10	20	5	10	20	5	10																																				
1000	$\frac{0.14}{885}$ [26.8] [27.8]	$\frac{0.01}{871}$ [18.4] [16.5]	$\frac{0.01}{825}$ [9.6] [9.6]	$\frac{1.21}{471}$ [21.0] [24.3]	$\frac{0.28}{400}$ [16.3] [17.2]	$\frac{0.02}{365}$ [10.9] [11.0]	$\frac{2.55}{43.1}$ [25.6] [34.9]	$\frac{0.66}{35.2}$ [24.0] [27.8]	2000	$\frac{0.29}{851}$ [30.2] [31.5]	$\frac{0.04}{815}$ [18.8] [19.1]	$\frac{0.01}{731}$ [11.4] [11.4]	$\frac{4.23}{374}$ [24.7] [30.6]	$\frac{0.85}{348}$ [19.5] [21.0]	$\frac{0.06}{284}$ [13.6] [13.8]	$\frac{0.59}{20.7}$ [48.3] [56.4]	$\frac{0.11}{8.5}$ [60.5] [54.0]	4000	$\frac{0.43}{792}$ [34.9] [36.5]	$\frac{0.08}{719}$ [22.3] [22.6]	$\frac{0.02}{574}$ [14.1] [14.2]	$\frac{8.41}{316}$ [30.4] [38.8]	$\frac{1.31}{264}$ [24.7] [27.0]	$\frac{0.08}{162}$ [19.0] [19.5]	—	—	—	—	6000	$\frac{0.57}{740}$ [38.4] [40.2]	$\frac{0.09}{636}$ [25.1] [25.6]	$\frac{0.03}{445}$ [16.7] [16.8]	$\frac{9.80}{269}$ [35.6] [45.6]	$\frac{1.32}{198}$ [29.9] [32.5]	$\frac{0.00}{75}$ [27.5] [27.5]	—	—	—	—	8000	$\frac{0.64}{692}$ [41.5] [43.4]	$\frac{0.14}{561}$ [27.7] [28.2]	$\frac{0.04}{335}$ [19.5] [19.7]	$\frac{10.18}{227}$ [40.5] [51.7]	$\frac{0.68}{141}$ [36.5] [39.1]	$\frac{0.02}{18}$ [49.3] [48.6]	—	—	—	—

^aFor each case the results are entered in the following form:

$$\frac{q_{\text{net}}(\text{real}, C_{\text{o,Gauss}}) - q_{\text{net}}(\text{real}, C_{\text{o,real}})}{q_{\text{net}}(\text{real}, C_{\text{o,real}})} \begin{bmatrix} C_{\text{o,Gauss}} \\ C_{\text{o,real}} \end{bmatrix}$$

Inserting this into Eq. 5-6 and taking the derivative with respect to C produces the condition for the optimal concentration ratio C_o as

$$0 = \frac{dq_{net}}{dC} = \frac{1}{C^2} \left(\frac{q_L}{(\rho \tau \alpha)} + X_S I_b - I_d \right) + \frac{d}{dC} \int_{-\infty}^{\infty} d\theta f(\theta) \frac{I_b}{\sigma_{tot} \sqrt{2\pi}} \exp \left(- \frac{\theta^2}{2 \sigma_{tot}^2} \right). \quad (5-9)$$

The integral is a function of $(\sigma_{tot} C)$ only. It is convenient to define a function

$$G(\sigma_{tot} C) = (\sigma_{tot} C)^2 \frac{d}{d(\sigma_{tot} C)} \int_{-\infty}^{\infty} d\theta f(\theta) \frac{1}{\sigma_{tot} \sqrt{2\pi}} \exp \left(- \frac{\theta^2}{2 \sigma_{tot}^2} \right) \quad (5-10)$$

because in terms of G and the critical intensity ratio X of Eq. 5-5 the optimization condition reads

$$\sigma_{tot} X = G(\sigma_{tot} C_o). \quad (5-11)$$

The function G has been evaluated numerically and is plotted versus $\sigma_{tot} C$ for different rim angles in Figure 5-1a for a cylindrical receiver and in Figure 5-1b for a one-sided flat receiver. To find the optimal concentration ratio C_o , one draws a horizontal line corresponding to the value of $\sigma_{tot} X$; the intersection of this line with the curve has the abscissa $\sigma_{tot} C_o$.

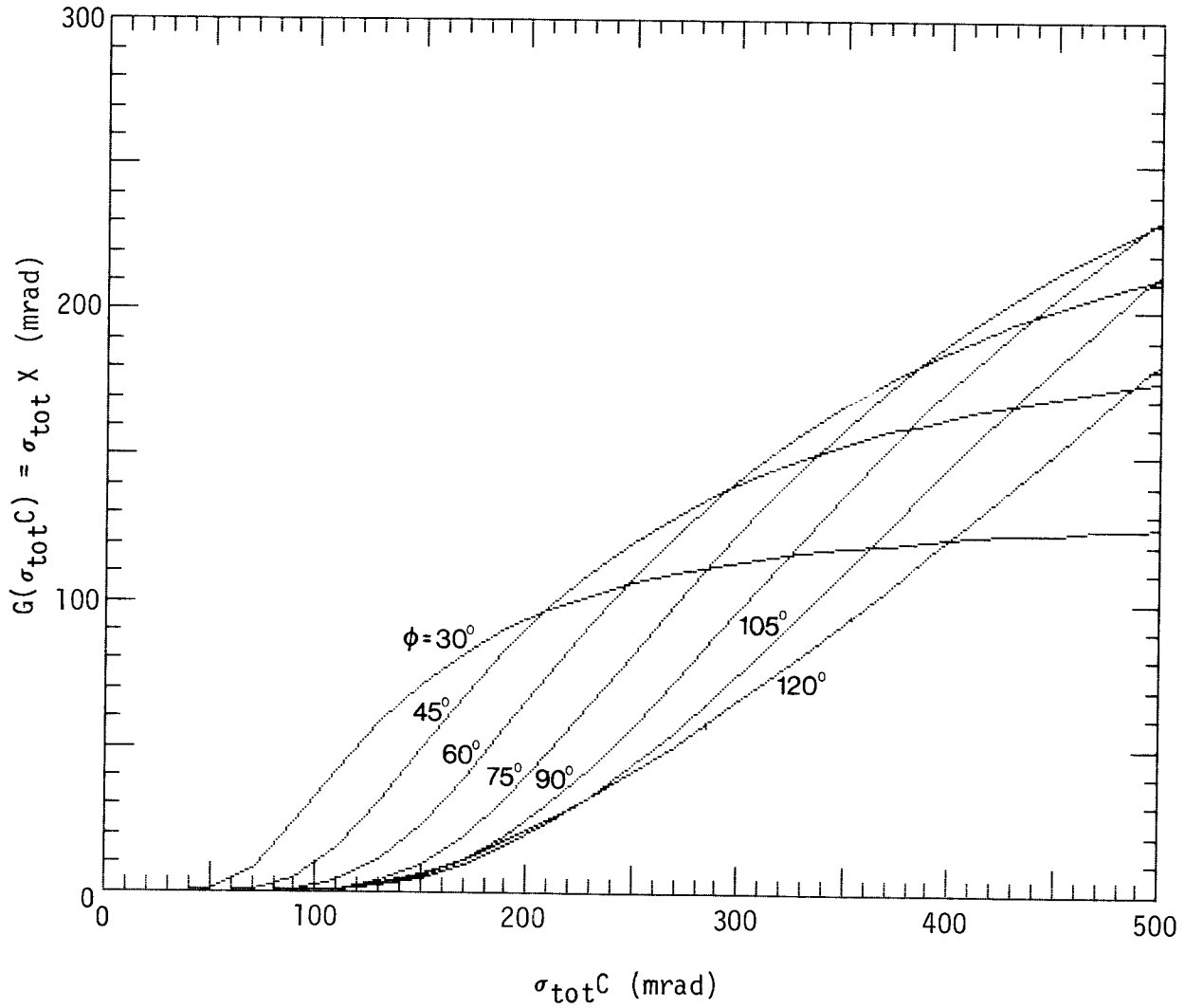


Figure 5-1a. THE CURVE $G(\sigma_{TOT}C)$ FOR FINDING THE OPTIMAL CONCENTRATION RATIO FOR DIFFERENT RIM ANGLES ϕ FOR A CYLINDRICAL RECEIVER.

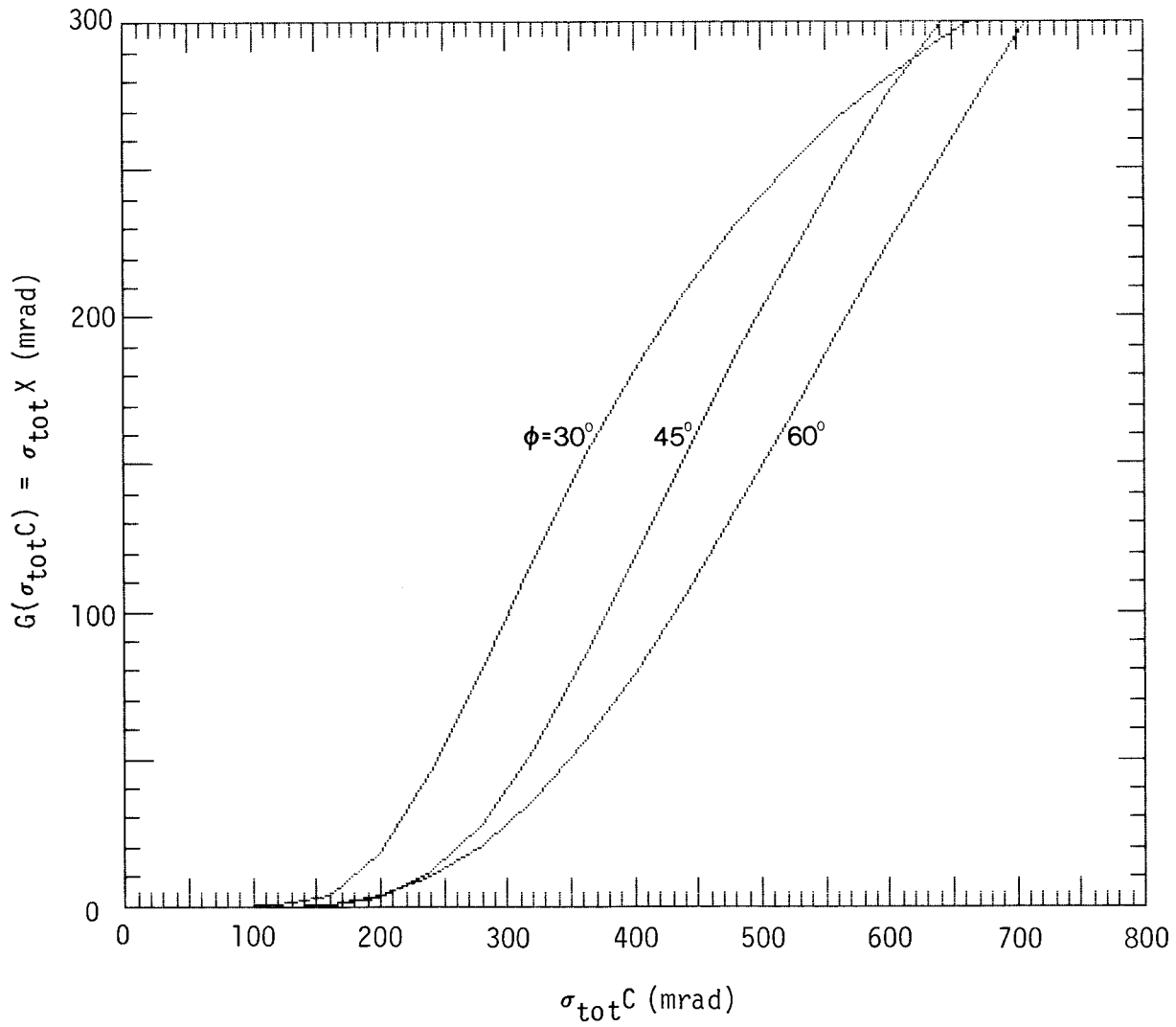


Figure 5-1b. THE CURVE $G(\sigma_{TOT}C)$ FOR FINDING THE OPTIMAL CONCENTRATION RATIO FOR DIFFERENT RIM ANGLES ϕ FOR A FLAT RECEIVER.



SECTION 6.0

EXAMPLES/USERS GUIDE

Demonstrated in this section is how the formulas and graphs developed in this paper can be used to design and optimize a parabolic trough concentrator, to calculate its thermal performance, and to evaluate its sensitivity to circumsolar radiation. The optimization is based on typical average insolation data [6] rather than on peak radiation at solar noon, as discussed in the Appendix.

6.1 OPTIMIZATION PHILOSOPHY

The performance of any solar energy system improves if the collector efficiency is increased, all other variables being constant. Therefore, the performance of the collector should be maximized independent of the rest of the system if such a step does not significantly increase the collector cost. The variables which affect collector performance fall into several groups:

- (1) operating conditions (insolation, tracking mode, operating temperature, flow rate, etc.);
- (2) properties of materials (reflectance, absorptance, etc.);
- (3) receiver design parameters (absorber shape, width of gap between absorber surface and glazing, etc.); and
- (4) concentrator geometry (concentration ratio C and rim angle ϕ).

The operating conditions may vary from installation to installation. On the other hand, cost reduction by mass production requires a certain amount of standardization. Thus it is preferable to design a solar collector which is approximately optimal for a range of typical operating conditions rather than for a specific application. The examples in this paper show that the optimum is sufficiently broad to permit much standardization without significant performance penalty.

If several candidate materials are available, the optimal choice has to be made by examining cost and performance for each case. As for the receiver design, one first has to select the generic type (flat or cylindrical, evacuated or nonevacuated). For an evacuated receiver a cylindrical absorber with a concentric glass envelope is probably the most reasonable choice, and the spacing between the absorber and glass envelope should be as small as is practical. For a nonevacuated receiver the spacing between absorber surface and glazing will usually be optimized if the corresponding Raleigh number is approximately 1500; in other words the spacing should be made as large as possible without initiating convection.

Once the receiver (type and size) and the materials have been chosen, one has to address the remaining set of variables, group (4). The concentration ratio C , i.e., the relative size of aperture and receiver, is particularly important. As C is increased, the heat loss per aperture decreases but so does the fraction of the incident solar radiation that is intercepted by the receiver. At the optimal concentration ratio the incremental heat loss equals the incremental loss of intercepted solar radiation. The optimization of C is carried out most conveniently by keeping the receiver size fixed while varying the aperture. Only a single number, the heat loss rate q_L (in W/m^2) per receiver surface area, is needed to characterize the thermal properties of the receiver.

For the optimization in this paper a standard set of operating conditions, variables in group (1), is assumed as a starting point. The selection of values for the variables in groups (2) and (3) is not addressed in this paper; rather a set of values is assumed as input.

Once the variables in groups (1) to (3) have been chosen, the optimization of concentration ratio and rim angle can be accomplished by the design procedure developed in this paper. In practice the mathematical optimum is not always the most desirable design because certain components, e.g., reflector sheets, may be available only in discrete sizes. Nonetheless, knowledge of the optimum is valuable as a guide in the selection of a practical design.

6.2 COLLECTOR PARAMETERS

Consider a long east-west-mounted parabolic trough reflector with a cylindrical receiver. The receiver has a selective coating and a glass envelope around it, as appropriate for operation in the $200^\circ C$ to $300^\circ C$ range [13]. It is assumed that the collector is characterized by the parameters listed in Table 6-1; they represent typical values for state-of-the-art technology. The entries under the contributions to beam spreading (optical error) are based on data reported by Sandia Laboratories for realistic materials and fabrication techniques [12,13]. The reflectance ($\rho = 0.85$) is typical of clean aluminum or dirty silver reflectors. The transmittance ($\tau = 0.88$) and the absorptance ($\alpha = 0.94$) are reasonable values when incidence angle effects are taken into account [14,15]. The product $(\rho\tau\alpha)$ will be reduced by dirt, but compensating improvement with antireflection coatings is possible. Present operating experience is insufficient to evaluate with confidence the effects of long-term environmental degradation, but preliminary data [17,18] indicate that dirt on a reflector reduces the specular reflectance by about 0.05 to 0.2 (depending on the cleaning cycle) with little change in σ_{specular} . A value of 0.70 for the all-day average reflectance-transmittance-absorptance product $\langle(\rho\tau\alpha)\rangle$ appears to be realistic. In any case only the product, not the individual factors, matters for the present purpose. At noon it will be higher and $(\rho\tau\alpha)_{\text{noon}} = 0.73$ is assumed [14]; the change in $(\rho\tau\alpha)$ with incidence angle should be measured, of course.

In many concentrating collectors part of the aperture is shaded by the receiver; this effect can be accounted for by a shading correction (X_S in this paper). In the case of a cylindrical receiver with glazing, an equivalent correction is needed for that fraction of

Table 6-1. COLLECTOR PARAMETERS

Parameter	Value
$\sigma_{\text{contour}\perp}$	2.5 mrad
$\sigma_{\text{contour}\parallel}$	2.5 mrad
$\sigma_{\text{specular}\perp}$	2.0 mrad
$\sigma_{\text{specular}\parallel}$	2.0 mrad
σ_{tracking}	2.0 mrad
$\sigma_{\text{displacement}}$	2.0 mrad
$\langle(\rho \tau \alpha)\rangle_{EW}$	0.70
$(\rho \tau \alpha)_{\text{noon}}$	0.73
d_{glass}	5.0 cm
d_{absorber}	2.5 cm
X_S	0.318
q_L	2000 W/m ²

the beam radiation incident on the aperture that passes through the glass envelope but misses the receiver. Due to refraction* it deviates so much from the design direction that it misses the receiver altogether on its return from the reflector. To find a typical value of X_S for the present configuration, assume a receiver tube of 2.5-cm outer diameter (d_{absorber}), surrounded by a glass tube of 5-cm outer diameter (d_{glass}). (With reasonable glass thickness this leaves an air gap of 1.0 cm, approximately optimal in terms of heat transfer because the corresponding Rayleigh number is just below the onset of convection.) X_S is given by the formula

$$X_S = \frac{d_{\text{glass}} - d_{\text{absorber}}}{\pi d_{\text{absorber}}} \quad (6-1)$$

and takes the value 0.318 in the present case (the factor of π inserted for consistent normalization to absorber surface area).

*Note parenthetically that refraction by a glass tube concentric with the absorber has no other effect on any of the calculations of this paper, as shown in Reference 10.

A crucial parameter is q_L , the heat loss per unit absorber surface area*. It must be interpreted as an average along the entire collector which is to be optimized. All the thermal properties of the collector enter only through this parameter, and, for the purpose of this paper, the detailed thermal properties are irrelevant; in particular, the precise value of emissivity and heat extraction efficiency, and the temperature nonuniformities are of no concern. The reader who is interested in calculating q_L is referred to the standard techniques in the heat transfer literature.** A rough and simple estimate for q_L can be obtained by extrapolating the flat-plate top heat loss coefficient in Fig. 7.4.4 of Reference 14. If collector test data are available, it is preferable to take for q_L the measured heat loss per unit of aperture area, multiplied by the geometric concentration ratio; such data have been reported, for example, in Reference 13. The value $q_L = 2000 \text{ W/m}^2$ in Table 6-1 is typical for the type of collector under consideration.

6.3 CHOICE OF RIM ANGLE

For cylindrical receivers the rim angle ϕ will be in the range of 80° to 120° . Figures 6-1a and b show the optimum to be so broad that the choice of rim angle can be determined by other considerations such as mechanical strength and ease of manufacturing.

In the literature two simple arguments have been given for determining ϕ_o . One argument is based on minimizing, for a given aperture area, the average path length from reflector to receiver, and it yields $\phi_o = 120^\circ$ [3]. The other argument [7,19] assumes complete capture of all rays within a prescribed angular range and results in $\phi_o = 90^\circ$. Neither of these arguments accounts for the detailed angular distribution of the radiation source, and hence it is not surprising that there is disagreement with the exact optimization. For the following discussion a 90° rim angle is assumed as a practical value.

6.4 OPTIMIZATION OF CONCENTRATION RATIO

The appropriate insolation values for optimization of the concentration ratio with respect to all-day average performance are calculated in the Appendix. They depend on incidence angle and hence on tracking mode, and they are listed in Table 6-2 for the most important configurations. The all-day average quantities are designated by angular brackets. They are based on an assumed operating time of 8 h/day. For other collection periods they can be recalculated by the methods in the Appendix.

*The heat loss term q_L is defined with respect to receiver rather than aperture area because conceptually this optimization procedure for the concentration ratio keeps the receiver fixed while varying the aperture.

**See, for example, Reference 16.

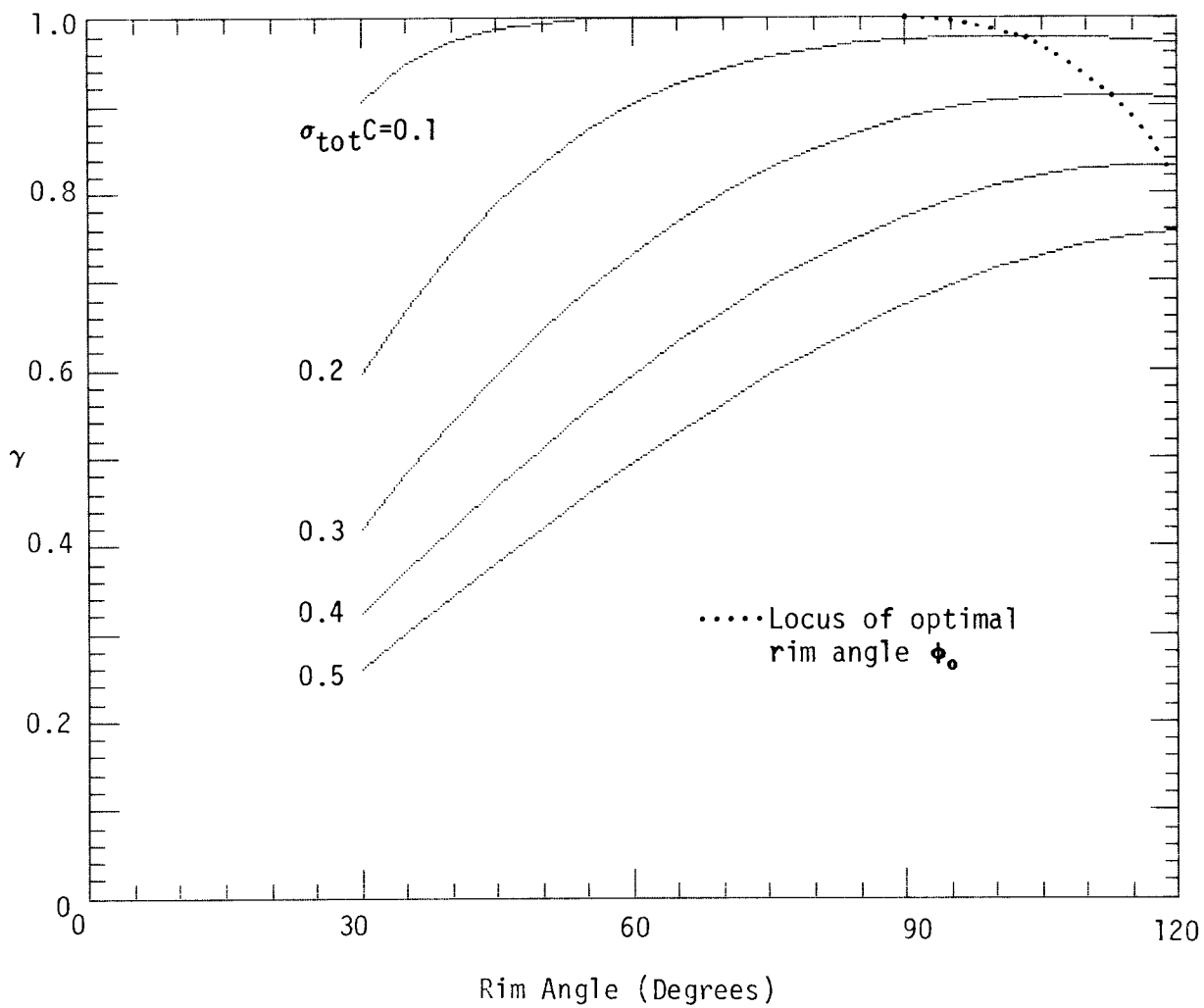


Figure 6-1a. INTERCEPT FACTOR γ VERSUS RIM ANGLE FOR PARABOLIC TROUGH WITH CYLINDRICAL RECEIVER.

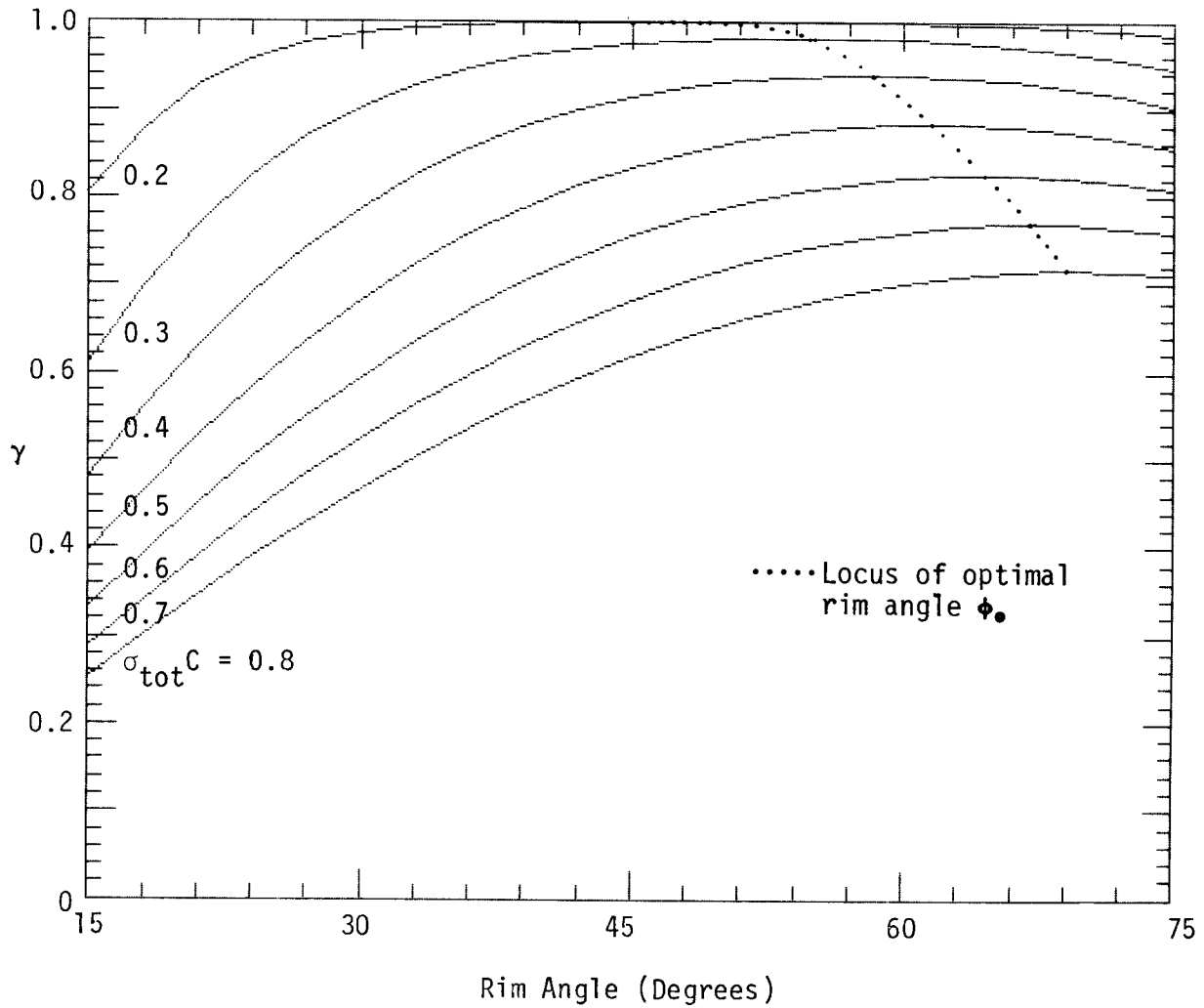


Figure 6-1b. INTERCEPT FACTOR γ VERSUS RIM ANGLE FOR PARABOLIC TROUGH WITH FLAT RECEIVER.

Table 6-2. TRACKING MODES AND ASSOCIATED SOLAR DATA

Solar Data	Tracking Mode				
	E-W Axis	N-S Axis Tilt = Latitude	N-S Axis Horizontal at 35° N latitude		
	Horizontal	Polar	Winter	Equinox	Summer
$\cos \Theta_{\text{noon}}$	1.0	$\cos \delta$	0.52	0.82	0.98
$\sigma_{\text{sun,noon}}$ (mrad) ^a	4.1	4.3 ^e	7.9	5.0	4.2
$\langle \cos \Theta \rangle$	0.77 ^b	0.96 ^e	0.63 ^b	0.89 ^c	0.99 ^d
$\langle \sigma_{\text{sun}} \rangle$ (mrad) ^a	5.0 ^b	4.3 ^e	6.6 ^b	4.6 ^c	4.2 ^d
$I_b \cos \Theta_{\text{noon}}$ (W/m ²)	865	830 ^e	460	710	825
$\langle I_b \cos \Theta \rangle$ (W/m ²)	665 ^b	750 ^{c,e}	490 ^b	670 ^c	720 ^d
$I_{d,\text{noon}}$ (W/m ²)	190	190	125	190	220
$\langle I_d \rangle$ (W/m ²)	160 ^b	140 ^c	95 ^b	140 ^c	160 ^d

^aAverage over typical sky conditions (circumsolar scans 1 through 10 in Table 4-1).

^bAll-day average based on 8 h/day.

^cAll-day average based on 10 h/day.

^dAll-day average based on 12 h/day.

^eIncludes all-year average of $\langle \cos \delta \rangle = 0.96$.

The steps of the calculation are entered into the worksheet in Table 6-3. First one computes the optical error derived in Section 2.0:

$$\begin{aligned} \sigma_{\text{optical}}^2 = & 4 \sigma_{\text{contour}_{\perp}}^2 + \sigma_{\text{specular}_{\perp}}^2 \\ & + \lambda(\Phi) \left(4 \sigma_{\text{contour}_{\parallel}}^2 + \sigma_{\text{specular}_{\parallel}}^2 \right) \\ & + \sigma_{\text{tracking}}^2 + \sigma_{\text{displacement}}^2 . \end{aligned} \quad (6-2)$$

The coefficient $\lambda(\Phi)$ represents the rim-angle-dependent contribution of longitudinal mirror errors to transverse beam spreading. It depends weakly on incidence angle and hence on tracking mode. $\lambda(\Phi)$ is given by Eq. 2-21 and Table 2-1. However, some simplification is permissible because this term is so small that its precise variation with Φ has negligible influence on the choice of optimal concentration ratio and rim angle. For the cases of greatest interest one can use the following approximation

$$\lambda(\Phi) = \begin{cases} 0 & \text{for normal incidence} \\ 0 & \text{for polar mount all-day average} \\ 0 & \text{for } \Phi \lesssim 45^\circ \text{ for east-west tracking axis all-day average} \\ 0.1 & \text{for } 80^\circ \lesssim \Phi \lesssim 110^\circ \text{ for east-west tracking axis all-day average.} \end{cases} \quad (6-3)$$

Hence, for the present example the all-day average optical error is as follows:

$$\begin{aligned} \langle \sigma_{\text{optical}} \rangle_{\text{EW}}^2 &= 1.1 \times (25 + 4) + 4 + 4 \text{ mrad}^2 \\ &= (6.3 \text{ mrad})^2. \end{aligned} \quad (6-4)$$

For the effective sun width the average $\sigma_{\text{sun,noon,average}} = 4.1$ mrad over circumsolar scans 1 through 10 (see Table 4-1) which appears to be representative of typical sky conditions. It is to be enlarged according to Eq. 2-12 to account for time-of-day variation:

$$\langle \sigma_{\text{sun}} \rangle_{\text{EW}} = \sqrt{1.5} \sigma_{\text{sun,noon,average}} = 5.0 \text{ mrad}. \quad (6-5)$$

The resulting total rms beam spread is given by

$$\begin{aligned} \langle \sigma_{\text{tot}} \rangle_{\text{EW}} &= \left(\langle \sigma_{\text{optical}} \rangle_{\text{EW}}^2 + \langle \sigma_{\text{sun}} \rangle_{\text{EW}}^2 \right)^{1/2} \\ &= 8.0 \text{ mrad}. \end{aligned} \quad (6-6)$$

The average critical intensity ratio is considered next:

$$\langle X \rangle = X_S + \left[\frac{q_L}{\langle (\rho \tau \alpha) \rangle} - \langle I_d \rangle \right] / \langle I_b \cos \Theta \rangle . \quad (6-7)$$

Table 6-3. OPTIMIZATION OF CONCENTRATION RATIO FOR PARABOLIC TROUGH WITH EAST-WEST AXIS: WORKSHEET

Parameter	Value	Reference
$\lambda(\phi)$	0.1	Eq. 6-3
$\langle \sigma_{\text{optical}} \rangle_{\text{EW}}$	6.3 mrad	Eq. 6-2 and 6-4
$\langle \sigma_{\text{tot}} \rangle_{\text{EW}}$	8.0 mrad	Eq. 6-6
$\langle X \rangle_{\text{EW}}$	4.37	Eq. 6-1 and 6-8
$\langle \sigma_{\text{tot}} \rangle_{\text{EW}} \langle X \rangle_{\text{EW}} = G(\langle \sigma_{\text{tot}} \rangle_{\text{EW}} C)$	35.0 mrad	Eq. 6-9
$\langle \sigma_{\text{tot}} \rangle_{\text{EW}} C_0$	218 mrad	Fig. 5-1a
C_0	27.3	Eq. 6-11

When the necessary items from Tables 6-1 and 6-2 are entered, it is found that

$$\langle X \rangle_{\text{EW}} = 0.318 + \left[\frac{2000}{0.70} - 160 \right] / 665 = 4.37. \quad (6-8)$$

If in Fig. 5-1a a straight line is drawn parallel to the abscissa ($\sigma_{\text{tot}} C$ axis), corresponding to the ordinate value

$$\langle \sigma_{\text{tot}} \rangle_{\text{EW}} \langle X \rangle_{\text{EW}} = 35 \text{ mrad}, \quad (6-9)$$

this line intersects the $\phi = 90^\circ$ curve at

$$\sigma_{\text{tot}} C = 218 \text{ mrad}. \quad (6-10)$$

This is the product of $\langle \sigma_{\text{tot}} \rangle_{\text{EW}}$ and the optimal concentration ratio C_0 for this collector. Thus the optimal concentration ratio which maximizes all-day efficiency is

$$C_0 = \frac{218 \text{ mrad}}{8 \text{ mrad}} = 27.3 \quad (6-11)$$

The efficiency has a broad maximum about C_0 and it is rather insensitive to the exact value of C_0 . Therefore, a range of concentration values from 25 to 30 can be recommended for this collector. Note that throughout this paper the geometric concentration is defined as the ratio of aperture area over receiver surface area. For a parabolic trough of aperture width D and absorber tube diameter d_{absorber} , the concentration is therefore

$$C = \frac{D}{\pi d_{\text{absorber}}}. \quad (6-12)$$

For an absorber tube diameter $d_{\text{absorber}} = 2.5$ cm, the optimal aperture width is

$$D = C_o \pi d_{\text{absorber}} = 214 \text{ cm.} \quad (6-13)$$

6.5 CALCULATION OF INTERCEPT FACTOR AND OPERATING EFFICIENCY

To calculate the efficiency it is important to know the intercept factor γ . It is defined as the fraction of the rays incident on the aperture that are intercepted by the receiver,*

$$\gamma = \frac{q_{\text{in}}}{I_b}, \quad (6-14)$$

and depends on σ_{optical} , sun shape, and concentration ratio C . The intercept factor is plotted versus $1/C$ for several values of σ_{optical} and for several sun shapes in Figure 4-2. Of particular interest is Figure 4-2d for the effective average sun shape. The solid lines give the result for the real sun shapes while the dotted lines are based on a Gaussian sun with the same rms width as the real sun. The assumption of a Gaussian sun shape has the advantage of reducing γ to a function of the quantity $(\sigma_{\text{tot}} C)$, thus facilitating graphical representation, as in Figure 4-1. The closeness of the solid and dotted lines in Figure 4-2 in the region of interest, i.e., $C \leq 30$, implies that the error in γ resulting from the Gaussian approximation is at most 1%. For example, if $\sigma_{\text{optical}} = 10$ mrad, the exact result for $C = 25$ and for the average sun shape, as indicated by the solid line in Figure 4-2d, is

$$\gamma_{\text{real}} = 0.920, \quad (6-15a)$$

The dotted line in Figure 4-2d (or equivalently Figure 4-1a) corresponding to the Gaussian approximation yields

$$\gamma_{\text{Gauss}} = 0.915. \quad (6-15b)$$

These numbers for the intercept factor are derived from Figure 4-2d and hence represent average values. The instantaneous intercept factor for extremely clear sky conditions at solar noon can be obtained in the same manner from Figure 4-2a for the narrow sun shape (circumsolar scan number 1 of Table 4-1).

In this section the efficiency

$$\eta = \frac{q_{\text{net}}}{I_b} \quad (6-16)$$

* γ is defined as a purely geometric quantity without regard to absorption or shading.

is calculated for peak and for all-day average conditions. The steps of the calculation are entered in the worksheet of Table 6-4. The efficiency can be expressed in terms of $(\rho \tau \alpha)$, γ , X , and C by

$$\eta = (\rho \tau \alpha) \left(\gamma - \frac{X}{C} \right). \quad (6-17)$$

The product $\eta_o = (\rho \tau \alpha) \gamma$ is called optical efficiency. To evaluate the all-day average operating efficiency $\langle \eta \rangle$, the parameters in Eq. 6-17 are based on the average sun shape and the average insolation level $\langle I_b \cos \Theta \rangle_{EW} = 665 \text{ W/m}^2$, as in Section 6.3. With the resulting values

$$\begin{aligned} \langle (\rho \tau \alpha) \rangle_{EW} &= 0.70, \\ \langle \gamma \rangle_{EW} &= 0.965 \text{ (read from Figure 4-1a, with } \langle \alpha_{tot} \rangle_C = 218 \text{ mrad)} \\ C_o &= 27.3, \text{ and} \\ \langle X \rangle_{EW} &= 4.37, \end{aligned}$$

the average efficiency is*

$$\langle \eta \rangle_{EW} = \langle (\rho \tau \alpha) \rangle_{EW} \left(\langle \gamma \rangle_{EW} - \frac{\langle X \rangle_{EW}}{C_o} \right) = 0.563. \quad (6-18)$$

*The only effect which has not been included is the spillover of radiation from collector ends in relatively short collectors. This end effect is installation-dependent and negligible for well-designed large collector fields. For short collectors (for example, test modules without end reflectors) this effect must be included by multiplying the intercept factor γ in Eq. 6-17 by an additional factor

$$\Gamma = 1 - \frac{f}{\ell} \left(1 + \frac{D^2}{48f^2} \right) \tan \Theta,$$

where f = focal length, ℓ = trough length, D = trough width, and Θ = incidence angle. This is discussed in Ref. 23.

Table 6-4. CALCULATION OF EFFICIENCY FOR COLLECTOR OPTIMIZED ACCORDING TO TABLE 6-3: WORKSHEET

Parameter	Value	Reference
C_o	27.3	Eq. 6-11
$\langle \rho \tau \alpha \rangle_{EW}$	0.70	Table 6-1
$\langle \sigma_{tot} \rangle_{EW} C_o$	218 mrad	Eq. 6-10
$\langle \gamma \rangle_{EW}$	0.965	Fig. 4-1a
$\langle X \rangle_{EW}$	4.37	Eq. 6-8
$\langle \eta \rangle_{EW}$	0.563	Eq. 6-18
$\sigma_{tot,noon}$	6.85 mrad	Eq. 6-19
$\sigma_{tot,noon} C_o$	187 mrad	
γ_{noon}	0.982	Fig. 4-1a
X_{noon}	3.40	Eq. 6-20
$(\rho \tau \alpha)_{noon}$	0.73	Table 6-1
η_{noon}	0.63	Eq. 6-21

For extremely clear sky (narrow sun shape) and a typical peak insolation value $I_{b,peak}$ of 865 W/m^2 , the results for this collector are

$$\sigma_{sun,narrow,noon} = 2.7 \text{ mrad, from Table 4-1, data set \#1;}$$

$$\sigma_{tot,noon} = \left(\sigma_{optical}^2 + \sigma_{sun,narrow,noon}^2 \right)^{1/2} = 6.85 \text{ mrad;} \quad (6-19)$$

$$\gamma_{noon} = 0.982, \text{ from Fig. 4-2a;}$$

and

$$X_{noon} = 0.318 + \left(\frac{2000}{0.7} - 191 \right) / 865 = 3.40. \quad (6-20)$$

The peak efficiency is

$$\eta_{noon} = (\rho \tau \alpha)_{noon} \left(\gamma_{noon} - \frac{X_{noon}}{C_o} \right) = 0.63. \quad (6-21)$$

for this collector.

This completes the calculations of optimal concentration ratio and operating efficiency. Next we consider the sensitivity of these results to changes in collector parameters and changes in operating conditions.

6.6 SENSITIVITY OF OPTIMIZATION TO CHANGES IN COLLECTOR PARAMETERS

Once a collector has been optimized for operation at a certain temperature, the deviation from optimal performance at different temperatures can be calculated. Optimization of concentration ratio is assumed for a heat loss parameter $q_L = 2000 \text{ W/m}^2$ as above, and the efficiency of this collector at lower or higher temperatures corresponding to $q_L = 1000 \text{ W/m}^2$ and $q_L = 3000 \text{ W/m}^2$ is then calculated.

These efficiencies are compared with those resulting from correct optimization for the new heat loss levels. Table 6-5 lists the respective efficiencies and concentration ratios for several values of the beam spread σ_{tot} calculated by using the Gaussian approximation.

The central column with $q_L = 2000 \text{ W/m}^2$ contains only one entry: $\eta(C = \dots) = \dots$. For the other two heat loss levels the top line lists η for C as optimized at $q_L = 2000 \text{ W/m}^2$, and the bottom line lists $\eta(C')$ with C' optimized for the new heat loss level.

Again the optimum is rather broad. For example, if a concentrator with $\sigma_{\text{optical}} = 10 \text{ mrad}$ is optimized for operation at a temperature corresponding to a heat loss $q_L = 2000 \text{ W/m}^2$, it will perform with $\eta = 0.6109$ at half the heat loss. If it is optimized for operation at $q_L = 1000 \text{ W/m}^2$ instead, the efficiency will be $\eta = 0.6156$, a gain of only half a percentage point. Therefore, it makes sense to market a single collector for a fairly wide range of operating temperatures and insolation levels rather than to try to optimize for each new application.

Table 6-5. SENSITIVITY OF OPTIMIZATION TO CHANGE IN HEAT LOSS PARAMETER q_L

σ_{tot} (mrad)	$q_L \text{ (W/m}^2\text{)}$		
	1000	2000	3000
5	$\eta(C = 37.92) = 0.6507$	$\eta(C = 37.92) = 0.6156$	$\eta(C = 37.92) = 0.5804$
	$\eta(C' = 33.15) = 0.6530$		$\eta(C' = 41.55) = 0.5820$
10	$\eta(C = 22.32) = 0.6109$	$\eta(C = 22.32) = 0.5511$	$\eta(C = 22.32) = 0.4913$
	$\eta(C' = 18.97) = 0.6156$		$\eta(C' = 25.01) = 0.4948$
20	$\eta(C = 13.75) = 0.5412$	$\eta(C = 13.75) = 0.4442$	$\eta(C = 13.75) = 0.3472$
	$\eta(C' = 11.17) = 0.5512$		$\eta(C' = 16.10) = 0.3547$

6.7 SENSITIVITY TO CIRCUMSOLAR RADIATION

The variation in efficiency with changing levels of circumsolar radiation can be evaluated by means of Figure 4-2. Only the intercept factor needs to be considered. Some examples are listed in Table 6-6. For each value of σ_{optical} and C , three numbers

Table 6-6. SENSITIVITY TO CIRCUMSOLAR RADIATION, EXACT CALCULATION AND GAUSSIAN APPROXIMATION. INTERCEPT FACTOR γ AS FUNCTION OF σ_{OPTICAL} AND C (FOR $\phi = 90^\circ$)^a

σ_{optical}	Concentration Ratio C					
	10		25		40	
5	1.0	(1.0)	0.99	(0.99)	0.94	(0.92)
	1.0	(1.0)	0.99	(0.99)	0.96	(0.96)
	1.0	(1.0)	0.95	(0.95)	0.88	(0.82)
10	1.0	(1.0)	0.92	(0.92)	0.76	(0.74)
	1.0	(1.0)	0.93	(0.93)	0.77	(0.77)
	1.0	(1.0)	0.89	(0.87)	0.72	(0.67)
20	0.97	(0.97)	0.67	(0.67)	0.47	(0.46)
	0.97	(0.97)	0.67	(0.67)	0.47	(0.47)
	0.96	(0.96)	0.66	(0.65)	0.46	(0.45)

^aEach entry contains

$\gamma_{\text{average,real}}$ ($\gamma_{\text{average,Gauss}}$)

$\gamma_{1,\text{real}}$ ($\gamma_{1,\text{Gauss}}$)

$\gamma_{11,\text{real}}$ ($\gamma_{11,\text{Gauss}}$)

for the average over circumsolar scans 1 through 10, for scan 1, and for scan 11 of Table 4-1.

are given (plus three more in parentheses). The first states the intercept factor averaged over circumsolar scans 1 through 10 which seems to correspond to normal operating conditions. (The scan numbers refer to the standard circumsolar profiles in Table 4-1.) The second entry corresponds to the narrow sun shape, scan 1, and the last entry to the wide sun shape, scan 11. The adjacent numbers in parentheses are obtained with the Gaussian approximation for the sun shape.

The following conclusions can be drawn. For concentration below 10 or for large optical errors, $\sigma_{\text{optical}} \gtrsim 20$ mrad, the collector performance is practically insensitive to circumsolar radiation under normal operating conditions, and the Gaussian approximation is quite acceptable for calculating the intercept factor. For the important case of concentrations around 25 and optical errors in the 5- to 10-mrad range, the intercept factor variation appears to be fairly small, about $\pm 1\%$, under normal conditions.

For the wider circumsolar scans the intercept decreases significantly, for example, by 4% for scan 11, but whether this is important in practice can only be decided when more information becomes available about the frequency distribution of the standard circumsolar profiles listed in Table 4-1.

6.8 OPERATION WITH NORTH-SOUTH AXIS

Calculation of yearly energy delivery [20,21,22] shows that in midlatitudes ($\lambda \approx 35^\circ$) an aperture tracking about the horizontal north-south axis receives approximately 15% more energy than one tracking about the east-west axis. Polar axis tracking approaches within 4% the radiation availability of a two-axis tracker, surpassing the horizontal east-west axis by about 30%. Despite its higher collection potential, the polar axis mount generally is believed to be impractical for large installations because of problems with wind loading and plumbing. Polar mount may, however, be desirable for small installations with relatively short collector modules, for example, for home heating.

The horizontal north-south axis suffers from large seasonal variation in output, resulting from variation not only of insolation but also of optical efficiency at low incidence angles. In order to get a quantitative assessment of these effects, it is useful to evaluate the performance of the collector discussed above if it is operated with a horizontal north-south instead of east-west axis. For its concentration ratio $C_o = 27.3$ is assumed, as optimized for east-west orientation. Table 6-7 lists all the steps of the calculations for the winter and summer solstices, in addition to the calculation for equinox.

The second to the last line of Table 6-7 shows that the intercept factor is fairly constant around 0.97 during spring and summer but drops to 0.926 at the winter solstice. This factor, coupled with a decreased ($\rho \tau \alpha$) product and lower beam insolation per aperture, leads to a significant drop in average operating efficiency from about 0.60 during the summer period to 0.50 at the winter solstice. Whether such low efficiency at a period of low available insolation is acceptable depends on the load profile for each particular application. This situation does not change if the collector is optimized specifically for north-south orientation rather than for east-west orientation as we have assumed. Repeating the optimization procedure for the north-south orientation (see Table 6-4) it is

found that the optimal concentration ratios differ only insignificantly: 26.6 for winter, 27.5 for equinox, and 27.7 for summer solstice. Therefore, a single concentration ratio in the range of 25 to 30 is optimal regardless of the orientation of the tracking axis.

Table 6-7. CALCULATION OF EFFICIENCY OF COLLECTOR WITH $C = 27.3$ (OPTIMIZED FOR EAST-WEST AXIS) IF OPERATED WITH HORIZONTAL NORTH-SOUTH AXIS

Parameter	Value			Reference
	Winter	Equinox	Summer	
$\langle(\rho \tau \alpha)\rangle_{NS}$	0.70	0.73	0.73	Table 6-1
$\langle\sigma_{sun}\rangle_{NS}$ (mrad)	6.6	4.6	4.2	Table 6-2
$\lambda(\emptyset)$	0.34	0.06	0	Eq. 2-21
$\langle\sigma_{optical}\rangle_{NS}$ (mrad)	6.85	6.22	6.10	Eq. 6-2
$\langle\sigma_{tot}\rangle_{NS}$ (mrad)	9.51	7.75	7.38	Eq. 6-6
$\langle I_b \cos\Theta \rangle_{NS}$ (W/m^2)	490	670	720	Table 6-2
$\langle I_d \rangle_{NS}$ (W/m^2)	95	140	160	Table 6-2
$\langle X \rangle_{NS}$	5.95	4.21	3.89	Eq. 6-7
$\langle\sigma_{tot}\rangle_{NS} C$ (mrad)	260	212	201	Fig. 5-1a
$\langle \gamma \rangle_{NS}$	0.926	0.966	0.971	Fig. 4-1a
$\langle \eta \rangle_{NS}$	0.50	0.59	0.61	Eq. 6-18

SECTION 7.0**REFERENCES**

1. Biggs, F.; Vittitoe, C. N. The Helios Model for the Optical Behavior of Reflecting Solar Concentrators. Albuquerque, NM: Sandia Labs.; SAND 76-0347.
2. Schrenk, G. M. Analysis of Solar Reflectors: Mathematical Theory and Methodology for Simulation of Real Reflectors. December 1963; GMC-AO-EDR3693.
3. Treadwell, G. W. Design Considerations for Parabolic Cylindrical Solar Collectors. Albuquerque, NM: Sandia Labs.; 1976; SAND 76-0082.
4. Cramer, H. Mathematical Methods of Statistics. Princeton, NJ: Princeton University Press; 1947.
5. Grether, D.; Hunt, A. Description of the LBL Reduced Data Base. Berkeley, CA: Lawrence Berkeley Laboratory; August 9, 1977.
6. Collares-Pereira, M.; Rabl, A. "The Average Distribution of Solar Radiation: Correlations between Diffuse and Hemispherical and between Daily and Hourly Insolation Values." Solar Energy. Vol. 22: pp. 155-164; 1979.
7. Rabl, A. "Comparison of Solar Concentrators." Solar Energy. Vol. 18: p. 93; 1976.
8. Pettit, R. B. "Characterization of the Reflected Beam Profile of Solar Mirror Materials." Solar Energy. Vol. 19: p. 733; 1977.
9. Butler, B. L.; Pettit, R. B. "Optical Evaluation Techniques for Reflecting Solar Concentrators." Society of Photo-optical Instrumentation Engineers (SPIE). Vol. 114, Optics Applied to Solar Energy Conversion: p. 43; 1977.
10. Rabl, A. "A Note on the Optics of Glass Tubes." Solar Energy. Vol. 19: p. 215; 1977.
11. Grether, D. F.; Hunt, A.; Wahlig, M. "Circumsolar Radiation: Correlations with Solar Radiation." Berkeley, CA: Lawrence Berkeley Labs.; Oct. 11, 1977.
12. Treadwell, G. (Sandia Labs.) Private communication.
13. Dudley, V. E.; Workhoven, R. M. Summary Report: Concentrating Solar Collector Test Results, Collector Module Test Facility. Albuquerque, NM: Sandia Labs.; May 1978; SAND 78-0815.
14. Duffie, J. A.; Beckman, W. A. Solar Energy Thermal Processes. New York, NY: John Wiley & Sons; 1974.
15. Kreith, F.; Kreider, J. F. Principles of Solar Engineering. New York, NY: McGraw-Hill; 1978.
16. Kreith, F. Principles of Heat Transfer. New York, NY: Intext Educational Publishers; 1973.

17. Pettit, R. B.; Freese, J. M.; and Arvizu, D. E. "Specular Reflectance Loss of Solar Mirrors Due to Dirt Accumulation." Presented at IES "Testing Solar Energy Materials and Systems" Seminar; May 22-26, 1978. Washington, DC: National Bureau of Standards.
18. Freese, J. M. Effects of Outdoor Exposure on the Solar Reflectance Properties of Silvered Glass Mirrors. Albuquerque, NM: Sandia Labs.; 1978; SAND 78-1649.
19. Tabor, H. "Stationary Mirror Systems for Solar Collectors." Solar Energy. Vol. 2: p. 27; 1958.
20. Treadwell, G. W. Low-temperature Performance Comparisons of Parabolic-trough and Flat-plate Collectors Based on Typical Meteorological Year. Albuquerque, NM: Sandia Labs.; 1978; SAND 78-0965.
21. Dickinson, W. C. "Annual Available Radiation for Fixed and Tracking Collectors." Solar Energy. Vol. 21: p. 249; 1978.
22. Collares-Pereira, M.; Rabl, A. Simple Procedure for Predicting Long-term Average Performance of Nonconcentrating and of Concentrating Solar Collectors. Argonne, IL: Argonne National Lab.; ANL-78-67. To be published in Solar Energy.
23. Gaul, H. W.; Rabl, A. "Incidence Angle Modifier and Average Optical Efficiency of Parabolic Trough Collectors." Golden, CO: Solar Energy Research Institute; 1979; SERI/TR-34-246R. To be published in ASME Journal of Solar Engineering. Vol. 1; 1980.

APPENDIX

TYPICAL INSOLATION VALUES FOR USE IN OPTIMIZATION

Optimization of concentrating collectors requires the input of the available solar radiation. Since a collector should perform well for a wide range of weather conditions, an exact optimization involves integration of collector output over insolation data for a long time period. Exact determination of rim angle and concentration ratio, however, is not necessary because the optimum is rather broad. Therefore, one can base the optimization on a single insolation value and sun shape, representing the average over typical operating conditions; i.e., the central eight to ten hours of a clear day.

The difference between such a simplified procedure and an exact optimization involves the replacement of the average of a product by the product of averages. A schematic example shows why such a procedure should be an excellent approximation in many solar energy calculations. Two sinusoidally varying terms are considered:

$$y_1 = a_1 + b_1 \cos \left(\frac{2 \pi t}{T} - \delta_1 \right) \quad (\text{A-1})$$

and

$$y_2 = a_2 + b_2 \cos \left(\frac{2 \pi t}{T} - \delta_2 \right) . \quad (\text{A-2})$$

The time average of the product $y_1 y_2$ over one period is

$$\langle y_1 y_2 \rangle = \langle y_1 \rangle \langle y_2 \rangle \left[1 + \left(\frac{b_1}{a_1} \right) \left(\frac{b_2}{a_2} \right) \cos (\delta_1 - \delta_2) \right] . \quad (\text{A-3})$$

The difference between $\langle y_1 y_2 \rangle$ and $\langle y_1 \rangle \langle y_2 \rangle$ is at most $(b_1 b_2)/(a_1 a_2)$. For example, if the relative magnitude of the oscillations about the average is $b_1/a_1 = 0.1 = b_2/a_2$, then the difference is at most 1%. If the frequencies differ, if the terms are out of phase, or if b_1 and b_2 represent random fluctuations uncorrelated with each other, the difference will be very small or vanish altogether.

One could expand the exact long-term average $q_{\text{net exact}}$ into a sum over multiple products similar to Eq. A-3. Some of the time variations of insolation and temperature are periodic (daily, yearly) while others are nearly random (clouds). The amplitudes of the variations are sufficiently small, typically less than 20%, and the terms are sufficiently uncorrelated to justify the approximation

$$\langle y_1 y_2 \rangle \approx \langle y_1 \rangle \langle y_2 \rangle .$$

To determine the appropriate average level of solar radiation, the Liu and Jordan correlations in the improved version recently published can be used [6]. The fundamental correlation parameter of this insolation model is the clearness index K_h , defined as the ratio of terrestrial (H_h) over extraterrestrial (H_0) daily hemispherical irradiation on a horizontal surface:

$$K_h = \frac{H_h}{H_0} . \quad (\text{A-4})$$

It is convenient to express time-of-day t and sunset time t_s as hour angles in radians from solar noon:

$$\omega = \frac{2 \pi t}{T} , \quad (\text{A-5})$$

$$\omega_s = \frac{2 \pi t_s}{T} = \arccos (-\tan \delta \tan \lambda) , \quad (\text{A-6})$$

where $T = \text{length of day} = 86,400 \text{ s}$, $\lambda = \text{latitude}$, and $\delta = \text{solar declination}$. The conversion between average irradiance $I \text{ (W/m}^2\text{)}$ and daily irradiation $H \text{ (J/m}^2\text{)}$ is given by

$$I_h = r_h H_h \quad (\text{A-7})$$

for the hemispherical component, and by

$$I_d = r_d H_d \quad (\text{A-8})$$

for the diffuse component, all measured on the horizontal surface. The factors r_d and r_h have been determined empirically. They are functions of time-of-day ω and of time of year (through ω_s) and are well represented by the following expressions:

$$r_d = \frac{\pi}{T} \left(\frac{\cos \omega - \cos \omega_s}{\sin \omega_s - \omega_s \cos \omega_s} \right) \quad (\text{A-9})$$

and

$$r_h = (a + b \cos \omega) r_d , \quad (\text{A-10})$$

with

$$a = 0.409 + 0.5016 \sin(\omega_s - 1.047)$$

and

$$b = 0.6609 - 0.4767 \sin(\omega_s - 1.047). \quad (\text{A-11})$$

The beam irradiance at normal incidence is given by

$$I_b = \frac{1}{\cos \Theta_h} (I_h - I_d), \quad (\text{A-12})$$

where

$$\cos \Theta_h = \cos \lambda \cos \delta (\cos \omega - \cos \omega_s) \quad (\text{A-13})$$

is the cosine of the incidence angle on the horizontal surface. In terms of K_h and H_o , Eq. A-12 can be written as

$$I_b = \frac{1}{\cos \Theta_h} \left(a + b \cos \omega - \frac{H_d}{H_h} \right) r_d K_h H_o, \quad (\text{A-14})$$

a form which is useful because the ratio H_d/H_h of diffuse over hemispherical irradiation is well correlated with K_h (see Eq. 6 and Figure 1a of Reference 6). The extraterrestrial irradiation H_o is given by

$$H_o = \frac{T}{\pi} I_o \cos \lambda \cos \delta (\sin \omega_s - \omega_s \cos \omega_s), \quad (\text{A-15})$$

where I_o = solar constant = 1353 W/m^2 . This formula neglects the seasonal variation (+3%) of the effective solar constant because only the year-round average is of interest.

Combining Eqs. A-9 and A-13 with Eq. A-15, most terms cancel, resulting in the simple expression

$$I_b = \left(a + b \cos \omega - \frac{H_d}{H_h} \right) K_h I_o. \quad (\text{A-16})$$

The analogous result for diffuse irradiance is

$$I_d = \cos \Theta_h \left(\frac{H_d}{H_h} K_h I_o \right). \quad (\text{A-17})$$

For present purposes I_d can be assumed to be isotropic and the brightness of ground and sky can be equated; hence, Eq. A-17 gives the diffuse irradiance on both the horizontal surface and the collector aperture for all tracking modes.

The yearly irradiation average is closely represented by its value at equinox, when

$$\begin{aligned} \delta &= 0 = \cos \omega_s, \\ a &= 0.6598, \text{ and} \\ b &= 0.4226. \end{aligned} \quad (\text{A-18})$$

Since concentrating collectors will operate only during periods of fairly high insolation, it is appropriate to take

$$K_h = 0.75, \quad (\text{A-19})$$

corresponding to clear days. The associated ratio of diffuse to hemispherical irradiation is

$$\frac{H_d}{H_h} = 0.23. \quad (\text{A-20})$$

At equinox the incidence angle Θ on a collector with an east-west tracking axis equals the hour angle ω ; hence, the product of beam irradiance and the cosine factor is

$$I_b(\omega) \cos \omega = \cos \omega (0.4298 + 0.4226 \cos \omega) I_o K_h. \quad (\text{A-21})$$

At solar noon, $\Theta = \omega = 0$ and we find a typical peak beam irradiance of

$$I_{b,\text{noon}} = 865 \text{ W/m}^2. \quad (\text{A-22})$$

Averaging Eq. A-21 over an operating period $2t_c$ yields

$$\langle I_b \cos \Theta \rangle_{\text{EW}, \omega_c} = \frac{1}{\omega_c} \int_0^{\omega_c} d\omega I_b(\omega) \cos \omega \quad (\text{A-23})$$

with

$$\omega_c = \frac{2 \pi t_c}{T}.$$

The result is

$$\langle I_b \cos \Theta \rangle_{\text{EW}, \omega_c} = [0.4298 \langle \cos \omega \rangle_{\omega_c} + 0.4226 \langle \cos^2 \omega \rangle_{\omega_c}] K_h I_o, \quad (\text{A-24})$$

with

$$\langle \cos \omega \rangle_{\omega_c} = \frac{\sin \omega_c}{\omega_c} \quad (\text{A-25})$$

and

$$\langle \cos^2 \omega \rangle_{\omega_c} = \frac{1}{2} + \frac{1}{2} \left(\frac{\cos \omega_c \sin \omega_c}{\omega_c} \right), \quad (\text{A-26})$$

which are listed in Table A-1 for various values of ω_c .

Table A-1. AVERAGE OF COSINE FACTORS FOR COLLECTOR WITH EAST-WEST TRACKING AXIS

	t_c (h)				
	2	3	4	5	6
ω_c (degrees)	30	45	60	75	90
$\langle \cos \omega \rangle_{t_c} = \frac{\sin \omega_c}{\omega_c}$	0.955	0.900	0.827	0.738	0.637
$\langle \cos^2 \omega \rangle_{t_c} = \frac{1}{2} + \frac{\cos \omega_c \sin \omega_c}{2 \omega_c}$	0.914	0.818	0.707	0.596	0.500

Taking $t_c = 4$ h as a typical cutoff time,

$$\langle I_b \cos \Theta \rangle_{EW} = 665 \text{ W/m}^2 \quad (\text{A-27})$$

is the average clear-day beam insolation per aperture area of a collector with an east-west tracking axis. This is not to be taken as an exact number; a range from 630 to 700 W/m^2 is reasonable.

The analogous results for the diffuse irradiance at equinox are

$$I_d = \cos \lambda \cos \omega \left(\frac{H_d}{H_h} K_h I_o \right) \quad (\text{A-28})$$

and

$$\langle I_d \rangle_{\omega_c} = \cos \lambda \langle \cos \omega \rangle_{\omega_c} \left(\frac{H_d}{H_h} K_h I_o \right). \quad (\text{A-29})$$

On a clear day, for $\lambda = 35^\circ$, this becomes

$$I_{d,\text{noon}} = 190 \text{ W/m}^2$$

and

$$\langle I_d \rangle_{t_c = 4 \text{ h}} = 160 \text{ W/m}^2. \quad (\text{A-30})$$

For a polar-mounted tracking collector the incidence angle Θ equals the declination δ at all times. To obtain an average yearly value of the beam insolation, Eq. A-16 is evaluated at equinox but $\cos \Theta$ is replaced by its year-round average

$$\langle \cos \Theta \rangle = \langle \cos \delta \rangle = 0.96. \quad (\text{A-31})$$

With a cutoff time $t_c = 4 \text{ h}$ and $K_h = 0.75$, this yields

$$\langle I_b \rangle_{\text{polar}, t_c = 4 \text{ h}} = 760 \text{ W/m}^2.$$

Document Control Page	1. SERI Report No. TR-34-092	2. NTIS Accession No.	3. Recipient's Accession No.
4. Title and Subtitle Optical Analysis and Optimization of Line Focus Solar Collectors		5. Publication Date September 1979	
7. Author(s) P. Bendt, A. Rabl, H. W. Gaul, K. A. Reed		6.	
9. Performing Organization Name and Address Solar Energy Research Institute 1536 Cole Blvd. Golden, Colorado 80401		8. Performing Organization Rept. No.	
		10. Project/Task/Work Unit No. 3432.30	
		11. Contract (C) or Grant (G) No. (C) (G)	
12. Sponsoring Organization Name and Address		13. Type of Report & Period Covered Technical Report	
		14.	
15. Supplementary Notes			
16. Abstract (Limit: 200 words) The optical analysis of a solar concentrator is usually carried out by means of a computer ray tracing, a microscopic method that provides an enormous amount of detailed information but obscures functional relationships. This paper describes a macroscopic approach that yields all the parameters needed for the optical design of line focus parabolic troughs in closed analytical form, requiring only minimal computation. The goal of the optical analysis is to determine the flux at the receiver as a function of concentrator configuration, receiver size, width of sun, and optical errors (e.g., tracking, reflector contour). All causes of image spreading are quantified as angular standard deviation. Ray tracing with a real reflector and a real sun is shown to be equivalent to convoluting the angular acceptance function of a perfect concentrator with an effective radiation source. This effective source, in turn, is obtained by convoluting the distribution function of optical errors with the angular profile of the sun. The problem is reduced to two dimensions by projecting the three-dimensional motion of the sun on the plane normal to the tracking axis. In this frame the apparent width of the sun increases as $1/\cos \theta$ with incidence angle θ . A formula and a simple graphical procedure are provided for finding the optimal geometric concentration ratio, maximizing net power output. In the last section, which is written as a self-contained users guide, the results are illustrated by specific examples.			
17. Document Analysis			
a. Descriptors Line Focus Collectors; Solar Collectors; Solar Concentrators; Optical Microscopy; Radiation Flux; Gauss Function; Sun; Optimization; Concentration Ratio; Concentrating Collectors			
b. Identifiers/Open-Ended Terms			
c. UC Categories UC-62a, 62b, 62e			
18. Availability Statement NTIS, U. S. Dept. of Commerce 5285 Port Royal Road Springfield, VA 22161		19. No. of Pages 73	
		20. Price \$5.25	